https://doi.org/10.5194/egusphere-2026-4826
Preprint. Discussion started: 25 August 2026


# Solute Release from Floodplains during Distinct Types of Inundation Events: Insights from Field Experiments and Reactive Transport Simulations

Zach Perzan[1], Kristin Boye[2], John R. Bargar[3], and Kate Maher[4]

[1]Department of Geoscience, University of Nevada Las Vegas, Las Vegas, NV, USA
[2]SLAC National Accelerator Laboratory, Menlo Park, CA, USA
[3]Environmental Molecular Science Laboratory, Pacific Northwest National Laboratory, Richland, WA, USA
[4]Department of Earth System Science, Stanford University, Stanford, CA, USA

**Correspondence:** Zach Perzan (zach.perzan@unlv.edu)

**Abstract.** Floodplains exert profound control on catchment water quality by transiently storing, transforming, and releasing solutes and particulate matter as they flow through the river corridor. These dynamic environments are shaped by periodic floods that increase hydrologic connectivity, linking shallow floodplain soils to groundwater and surface water and driving abrupt shifts in solute mobility. While floodplain inundation is often assumed to flush accumulated solutes toward groundwater and surface water, floods can arise through several different mechanisms — including overbank flow, rising groundwater levels, and rainfall- or snowmelt-induced ponding — each of which likely has a distinct impact on solute transport. Here, we combine field observations with reactive transport simulations to evaluate how distinct forms of inundation impact solute mobilization from floodplains. Results from a dye infiltration experiment reveal that precipitation-driven, top-down inundation events (such as rainfall in excess of infiltration capacity) induce preferential flow through macropores. This floodwater bypasses the soil matrix and results in minimal solute exchange. In contrast, observations from a groundwater-driven, bottom-up flood show rapid increases in solute concentrations as groundwater rose into the soil profile and dissolved evaporites within the soil matrix. To generalize beyond these field observations, we use dual permeability reactive transport simulations to test how inundation type, magnitude, and timing affect net solute exchange between the soil and underlying aquifer. Simulations show that groundwater-driven, bottom-up floods drive a net gain of solutes from the aquifer to the floodplain. Top-down floods, on the other hand, lead to solute loss from the floodplain to the aquifer, but this loss can be outweighed by summer plant water demand, which limits downward percolation of floodwater. Collectively, these results reveal that floodplain inundation cannot be interpreted as a simple flushing process. Instead, net solute exchange depends on the type of inundation event, the extent of preferential flow, and the seasonal timing of flooding with respect to plant transpiration.

## 1 Introduction

Floodplains are critical interfaces where surface water, groundwater, soils, and vegetation interact. In these dynamic environments, periodic floods connect water from the river channel with pools of reactive species stored within the floodplain. Though these events are brief, they can trigger biogeochemical “hot moments” that have an outsized impact on nutrient cy-

https://doi.org/10.5194/egusphere-2026-4826
Preprint. Discussion started: 25 August 2026


cling, contaminant mobility, and greenhouse gas production within the watershed (Junk et al., 1989; Amoros and Bornette, 2002; Tockner and Stanford, 2002; McClain et al., 2003; Bernhardt et al., 2017). Understanding how inundation alters solute storage and export is therefore essential for managing water quality and riparian health (Bayley, 1995).

At river reach and catchment scales, flood-induced solute cycling is often interpreted through the competing effects of enrichment and dilution. Observed concentration–discharge (C–Q) patterns are typically classified as either dilution (decreasing C with increasing Q), enrichment (increasing C with increasing Q), or chemostasis (constant C with increasing Q). For solutes concentrated in shallow soils such as dissolved organic carbon and nitrate, increases in river discharge often coincide with increases in solute concentrations within the stream (e.g., Hornberger et al., 1994; Boyer et al., 2000); this enrichment pattern is often interpreted to represent the flushing of stored solutes to the river channel (Johnson et al., 1969; Evans and Davies, 1998; Musolff et al., 2015). In other instances, increases in discharge are accompanied by decreases in solute concentrations, reflecting dilution of in-stream solutes by relatively dilute event water (e.g., Johnson et al., 1969; Hall, 1971; Zhi et al., 2019; Fang et al., 2024). Still other watersheds exhibit chemostatic C–Q relationships, in which stream concentrations remain constant with changes in discharge (Godsey et al., 2009; Creed et al., 2015).

However, river chemistry integrates contributions from diverse sources, including hillslopes, riparian zones, floodplains, and groundwater. The relative contribution of each source changes as inundation increases lateral and vertical connectivity across the landscape, activating source waters with contrasting chemistry (Herndon et al., 2015; Zhi et al., 2019; Allgeier et al., 2021; Xiao et al., 2021). Floodplains are a complex component of this system because they can store and transform water and solutes over timescales that differ from both hillslopes and upstream tributaries (Bouchez et al., 2012; Wohl, 2021). In addition, floodplains host large pools of reactive solutes and particulates (Wohl, 2021; Babey et al., 2024) and may therefore contribute disproportionately to reach-scale C-Q signals (Sawyer et al., 2014; Carroll et al., 2018; Rose et al., 2018).

In spite of increasing high-resolution C-Q data, interpreting the impact of floodplains on C–Q relationships remains challenging because discharge alone does not determine how floodwater interacts with the floodplain. One source of complexity is that inundation can arise from multiple sources (Mertes, 2000). In the traditional conceptual model of a flood, surface runoff initiates within low order streams, which then flow into tributaries and converge into the main channel. Inundation occurs when river stage rises high enough to breach the banks and spill onto the floodplain. However, inundation can arise through other means. For example, precipitation that falls directly onto the floodplain can pond on the surface when the rainfall rate exceeds the infiltration rate (Mertes, 2000; Day et al., 2008; Meyer Oliveira et al., 2024). Moreover, groundwater levels in floodplain aquifers are often tightly coupled with river stage (Hurr, 1981; Sophocleous, 1991; Bates et al., 2000; Burt et al., 2002; Jung et al., 2004) and the water table in the floodplain can rise to the surface without overbank flow, resulting in groundwater-driven flooding (e.g., Bradley et al., 2010; Macdonald et al., 2012; Buffin-Bélanger et al., 2016; Abboud et al., 2018). Thus, two inundation events could exhibit similar properties on the surface — identical depths of ponded water — even though they might arise from different mechanisms.

A second source of complexity is that inundation does not necessarily produce uniform wetting or reaction fronts within floodplains. In most soils, ponded water percolates downward via preferential flow along root channels, soil cracks, worm burrows, and other macropores (Beven and Germann, 1982; Hillel, 1987; Flury et al., 1994; Jarvis, 2007; Nimmo, 2021).

https://doi.org/10.5194/egusphere-2026-4826
Preprint. Discussion started: 25 August 2026


Reactive solutes are often stored in relatively immobile porewater — such as dead-end pores, soil aggregates, and fine-grained sediment lenses (Coats and Smith, 1964; Rezanezhad et al., 2016; Babey et al., 2022; Lacroix et al., 2023) — and preferential flow allows floodwater to bypass these zones. As a result, inundation might increase hydrologic connectivity without mobilizing solutes. Even where floodwater contacts reactive storage zones, the magnitude of solute release depends on other factors such as residence time and reaction rates, which control the extent of mineral dissolution, desorption, and organic matter oxidation (White and Brantley, 2003; Maher, 2010; Thompson et al., 2011). Thus, despite the common assumption that floods flush accumulated solutes from floodplains, it remains unclear how these processes control net solute exchange.

The goal of this study is to determine how distinct mechanisms of inundation impact solute export from floodplain soils. Focusing on a semi-arid floodplain along the Little Wind River (Wyoming, U.S.A.), we present results from field experiments that captured changes in water flow and porewater chemistry during two distinct types of inundation events. To quantify solute fluxes under a broader range of floods than were observed in the field, we performed reactive transport simulations that investigated the effects of inundation type, magnitude, and timing on net solute export. This approach provides a process-based framework for interpreting when floods promote solute retention or mobilization, identifying mechanistic controls that apply to many other floodplain systems.

## 2 Drivers of inundation on floodplains

For the purposes of this work, we define floodplain inundation as the presence of ponded water on the floodplain surface, which can arise from multiple mechanisms (Fig. 1). In connected stream–aquifer systems, the water table is approximately level with river stage during baseflow and, if it is a gaining system, groundwater in the floodplain aquifer flows towards the stream (Fig. 1a). During the first type of inundation event (Fig. 1b), a gradual rise in river stage drives a rise in the water table within the floodplain. If river stage rises above the ground surface elevation without overtopping adjacent levees, the floodplain can be inundated with water sourced entirely from the underlying aquifer. This type of inundation, a form of groundwater flooding, is driven by pressure transmission through the saturated zone that has been referred to as a "groundwater floodwave" (Buffin-Bélanger et al., 2016) or a "flow pulse" (Meyer Oliveira et al., 2024). Because water is delivered to the soil from below, we refer to this type of flooding as bottom-up inundation.

In the second type of event, which we refer to as top-down inundation, ponded water is supplied directly to the floodplain surface, such as from intense rainfall or melting snow. If the rainfall or snowmelt rate exceeds the infiltration rate, water ponds on the surface, infiltrates into the soil, and gradually percolates to the water table (Fig. 1c). Top-down inundation can also occur from sudden changes in river discharge, such as when river stage rises rapidly and overtops levees before the water table in the floodplain has time to rise in response (Fig. 1d).

In practice, floodplain inundation can be driven by a combination of these two mechanisms, such as when snowmelt or an areally extensive precipitation event deliver water both to the local floodplain (causing water to pond on the surface, as during top-down inundation) and to the upstream watershed (driving an increase in river stage, as during bottom-up inundation). The balance between these two processes depends on factors such as storm intensity, catchment size, floodplain topography, and

https://doi.org/10.5194/egusphere-2026-4826
Preprint. Discussion started: 25 August 2026


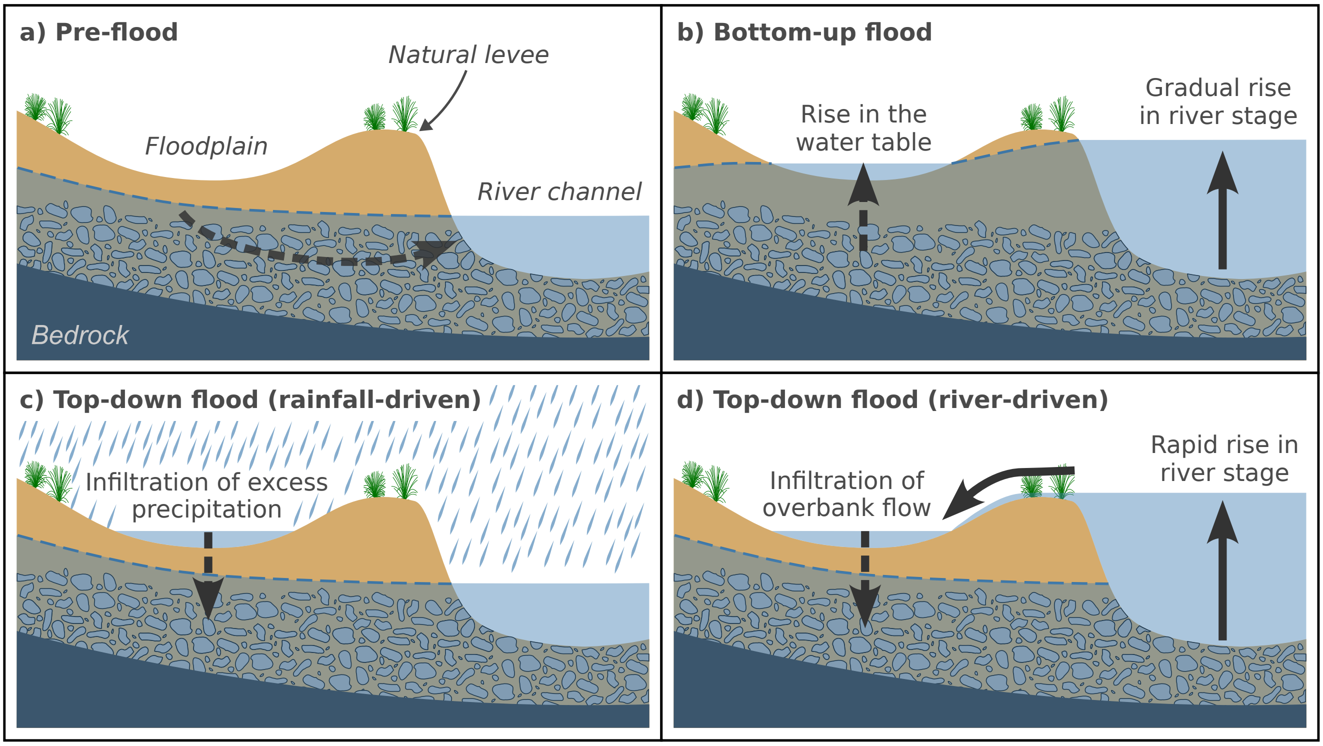


**Figure 1.** Conceptual diagram for different drivers of inundation along a floodplain in a connected stream–aquifer system. Before a flood (a), river stage is low and groundwater flows towards the river channel. During a bottom-up flood (b), river stage rises slowly, driving a concurrent rise in the water table and fully saturating the soil profile. If the river rises above the floodplain without spilling over adjacent levees, the land surface is inundated entirely from below. During a rainfall-driven, top-down flood (c), excess precipitation accumulates on the floodplain and infiltrates into the soil while the water table is at depth. A river-driven top-down flood (d) is triggered by a rise in river stage that is large enough to overtop adjacent levees and fast enough that the water table does not have time to respond. Ponded water then infiltrates through the soil to the water table. Note that mixed flood types (e.g., a rise in river stage during intense precipitation) can occur as well.

the hydraulic connectivity between the river and the floodplain. For ease of interpretation, we do not consider mixed flooding events and, in the remainder of this paper, we instead focus on pure bottom-up and top-down inundation.

## 3 Methods

### 3.1 Site description

95 The study site consists of a semi-arid floodplain along the Little Wind River near Riverton, Wyoming, USA. The Little Wind River is a 7th-order river (Strahler stream order) with a total drainage area of 4,505 $\mathrm{km}^2$, much of which comprises the southern portion of the Wind River Range. The floodplain experiences a cold semi-arid climate (Köppen classification BSk) character-

https://doi.org/10.5194/egusphere-2026-4826
Preprint. Discussion started: 25 August 2026


ized by cold winters and hot summers with low annual precipitation (~23 $\mathrm{cm\,yr^{-1}}$) and high annual potential evapotranspiration (~108 $\mathrm{cm\,yr^{-1}}$). Most precipitation occurs in the spring (April–July) and early fall (September–October). Vegetation across the floodplain consists of grasses, forbs, and shrubs (Picel, 2021), including sweetgrass (Hierochloe spp.), wheatgrass (Agropyron spp.), whitetop sulfur (Eriogonum umbellatum), sagebrush (Artemisia spp.), and rabbitbrush (Ericameria spp. and Chrysothamnus spp.).

As with many arid and semi-arid floodplains, the Little Wind River floodplain experiences seasonal inundation from multiple sources, including from local precipitation that exceeds soil infiltration capacity and from overbank flow during increases in river stage. The river is incised and bounded by a natural levee, which separates the active channel from the adjacent floodplain. Floods vary in frequency and duration, with flashy, storm-driven events lasting hours to days and broader snowmelt-driven floods lasting weeks.

The floodplain hosts a shallow, unconfined aquifer that consists of 3–4 m of coarse sand and gravel overlain by 2 m of loess deposits (Fig. 2). During baseflow, the water table is typically 1.2–1.5 m below the ground surface, though water levels change seasonally due to fluctuations in river stage. For most of the year, groundwater in the unconfined aquifer flows towards the Little Wind River, though the hydraulic gradient reverses seasonally with increases in river stage (Dam et al., 2015; Tolar et al., 2020; Thiros et al., 2021). Soil pits reveal abundant roots in the upper 0.5 m of the soil profile, with decreasing abundance down to 1.6 m (Fig. 4). Within 0.5 m of the surface, soils contain abundant evaporite minerals; previous X-ray diffraction work (Looney et al., 2014) identified blödite [$Na_2Mg(SO_4)_2 \cdot 4\,H_2O$] as the dominant evaporite mineral, with lesser concentrations of halite (NaCl), thenardite ($Na_2SO_4$), and mirabilite ($Na_2SO_4 \cdot 10\,H_2O$).

The Little Wind River floodplain has been instrumented with a variety of field equipment from past research at the site (White et al., 1984; Dam et al., 2015; Perzan et al., 2021; Paradis et al., 2022; Perzan and Chapin, 2023; Rasmussen et al., 2025). This includes four profiles of time-domain reflectometers installed to monitor changes in water content within the soil (Tolar et al., 2020). In addition, the Department of Energy maintains a network of monitoring wells equipped with pressure transducers to record changes in groundwater level and the U.S. Geological Survey operates a streamgage 4 km downriver of the floodplain.

### 3.2 Soil dye test

To assess subsurface flow patterns during surface ponding events, we conducted a dye infiltration test in June 2018. First, an infiltration ring with a diameter of 71 cm was inserted into the soil to a depth of 10 cm and bentonite clay was packed around the outside of the ring to limit leaks. The soil surface inside the infiltration ring, including soil cracks, was kept intact. Next, a 55-cm ponding pulse of dye-amended water was applied to the infiltration ring. This ponding depth was chosen to mimic the maximum potential surface ponding event that might occur at this site. The food-grade dye Brilliant Blue FCF was added to the inundation water at a concentration of 12 $\mathrm{g\,L^{-1}}$. Brilliant Blue FCF is a common dye used to study preferential flow in soils (Flury et al., 1994) and was chosen due to its low toxicity and its high visibility in soil.

One day after inundation, the soil was excavated in a series of horizontal and vertical cross-sections to examine flow patterns. Four 60 cm by 60 cm vertical cross-sections were prepared at 0, 10, 20, and 30 cm from the edge of the inundation ring (Fig.

https://doi.org/10.5194/egusphere-2026-4826
Preprint. Discussion started: 25 August 2026


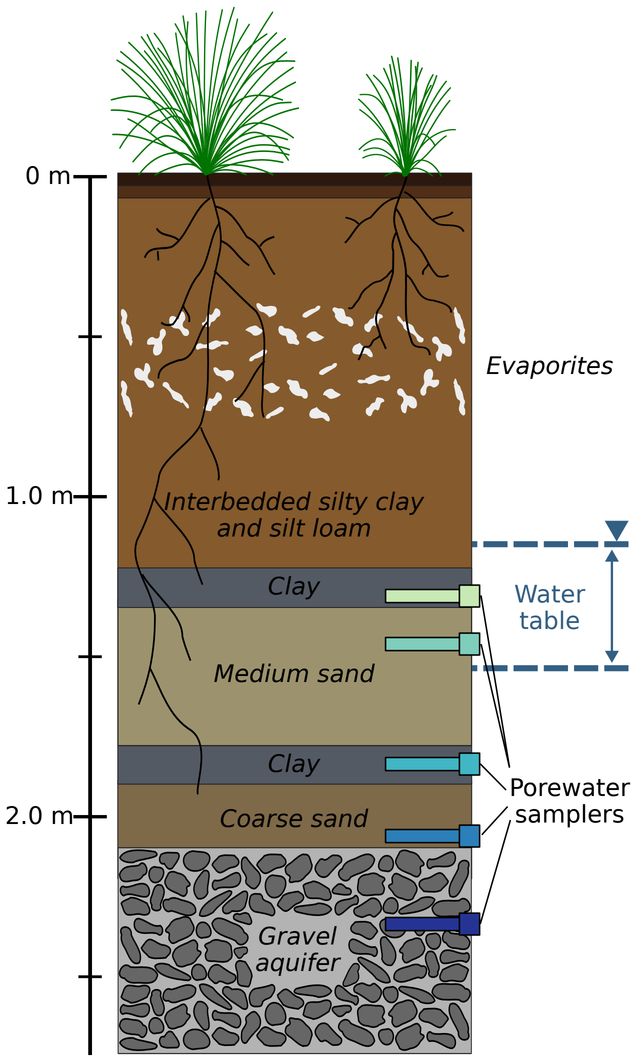


**Figure 2.** Simplified soil profile at the Little Wind River floodplain. The upper 1.3 m of the soil contains interbedded silty clay and silt loam with extensive evaporites at approximately 0.5 m depth. Thin clay lenses are found deeper in the soil profile and are separated by pockets of sand. Porewater samplers are colored by depth, with colors corresponding to the solute concentrations plotted in Fig. 4.

S1). Subsequently, five 60 cm by 60 cm horizontal cross-sections were prepared at 10, 20, 30, 40, and 50 cm depth immediately below the inundation ring (Fig. S1). All sections were carefully prepared with hand tools to avoid damage to soil structures and loose particles were removed to reveal macropore openings (Weiler and Flühler, 2004). Each section was then photographed using the procedure of Forrer et al. (1999). To limit color and lighting differences between photos, a white light tent was placed over the soil pit and a color scale was included in each photo for color-correction. All images underwent standard

https://doi.org/10.5194/egusphere-2026-4826
Preprint. Discussion started: 25 August 2026


post-processing procedures (Weiler and Flühler, 2004; Cey and Rudolph, 2009), including geometric correction, gray-value interpolation, background subtraction, color adjustment, histogram rectification, and final dye classification.

### 3.3 Water sampling and geochemical analyses

To monitor solute changes during natural floods, we collected soil porewater samples from March to October 2019 and quantified key anions ($Cl^-$, $SO_4^{2-}$, $NO_3^-$ and $PO_4^{3-}$) and metals/metalloids (Al, As, Ba, Ca, Cr, Cu, Fe, K, Mg, Mn, Mo, Na, Ni, Pb, Rb, S, Se, Si, Sr, U, V, and Zn). A gallery of porewater samplers was installed at 6 depths throughout the soil profile in November 2018. Within the vadose zone (70, 140, and 150 cm depths), porewater samplers (5 cm long, 0.15 µm pore size rhizons, Rhizosphere Research Products) were installed in an auger hole backfilled with original sediment. Below the water table (170, 208, and 221 cm depths), 6-mm-diameter tube wells with a 10 cm screen length (SedPoint Samplers, MHE Products, East Tawas, Michigan, USA) were installed with a dedicated insertion tool. Samples were collected approximately monthly in the spring and fall, weekly during the summer, and every 2 days during the June flood event. Porewater samples were immediately filtered at 0.22 µm and injected into pre-evacuated and crimp-sealed serum vials. Samples for metal concentrations were additionally acidified to pH 2 with ultrapure nitric acid. All samples were shipped on ice and stored at 2°C prior to analysis.

Concentrations of Ca, Fe, K, Mg, Na, S, and Si were analyzed on an inductively coupled plasma optical emission spectrometer (iCAP 6300 ICP-OES, Thermo Fisher Scientific, Cambridge, United Kingdom), while concentrations of all remaining metals/metalloids were analyzed by inductively coupled plasma mass spectrometry (XSERIES 2 ICP-MS, Thermo Fisher Scientific). All anion concentrations were measured via ion chromatography (Dionex ICS 6000 Ion Chromatograph, Thermo Fisher Scientific).

### 3.4 Reactive transport simulations

#### 3.4.1 Model parameterization

While field observations reveal the occurrence of macropore flow and solute release during floods, they provide limited spatial and temporal coverage, making it difficult to generalize across a wide array of hydrologic and geochemical conditions. To study these processes across a broader range of flood intensities, we developed reactive transport simulations of flood-induced solute flushing at the Little Wind River floodplain. We use the reactive transport code MIN3P (Mayer et al., 2002), which solves coupled flow and reactive transport equations in variably saturated media using a global implicit approach. The original MIN3P code has been extended to simulate dual-permeability flow and solute transport (Javadi, 2019; Jia et al., 2023, 2025) using the mathematical description of Gerke and Genuchten (1993). The code has undergone extensive benchmarking (Mayer and MacQuarrie, 2010; Mayer et al., 2015; Javadi, 2019) and has been successfully applied to flood propagation problems in the past (e.g., Perzan and Maher, 2024). Because the complete numerical formulation for MIN3P can be found elsewhere (Mayer et al., 2002, 2012), the governing equations are not reproduced here.

The 1D model domain consists of a 1.5-m soil column discretized into 150 grid cells with uniform thickness of 0.01 m. The domain is divided into dual continua that represent both the soil matrix and soil macropores, with exchange parameters governing water and solute mass transfer between the two (Fig. S2). Water exchange between the macropores and the matrix is calculated using the head difference between the two domains, the effective hydraulic conductivity of the matrix–macropore interface, and parameters describing the geometry of the macropores. Solute exchange between the two domains is computed as the sum of the advective solute flux — which depends on the rate of water transfer and upgradient concentrations — and the diffusive solute flux, which depends on the concentration gradient across the two domains and the effective diffusion coefficient near the matrix–macropore interface. A more detailed description of the governing equations is included in the Supplementary material (Text S1).

Based on field observations, soil macropores are assumed to extend from the surface down to 1.5 m depth and account for 5% of the total porous medium. We use the van Genuchten-Mualem formulation of the soil water retention and relative permeability curves (Mualem, 1976; van Genuchten, 1980). All dual permeability and soil hydraulic function parameters can be found in the Supplementary Material (Tables S1–S2).

Plant water demand plays a key role in both solute cycling and evaporite formation in floodplain soils. During the growing season (late spring and summer), transpiration can drive upward flow within the soil, a process that turns off in the fall after plant senescence. To simulate these processes in MIN3P, we use the root water uptake function of Battaglia and Sands (1997), which reduces transpiration non-linearly as a function of soil moisture. We parameterize the root water uptake function to fit water- and salinity-limited transpiration data for wheatgrass (Skaggs et al., 2006), which is prevalent across the Little Wind River floodplain. Soil pits revealed the presence of plant roots down to 2 m depth, with the highest root mass in the upper 0.5 m of soil. To represent this vertical root distribution, we assume that root length density decreases exponentially with depth (Gale and Grigal, 1987), using typical distributions observed in grasslands (Jackson et al., 1996).

The geochemical system includes 11 primary species ($H^+$, $Na^+$, $Mg^{2+}$, $Ca^{2+}$, $H_4SiO_4$(aq), $CO_3{}^{2-}$, $SO_4{}^{2-}$, $Cl^-$, and three artificial conservative tracers), 17 secondary species, one gas ($CO_2$), and four minerals (quartz, calcite, gypsum and blödite). These four minerals were chosen because they have all been observed in field samples (Looney et al., 2014) and because they span a broad range of solubilities and reaction rates in soils. We use inert tracers to track the movement of three different sources of water — antecedent soil moisture, floodwater, and groundwater from the underlying aquifer — throughout the domain. All intra-aqueous reactions are assumed to be at equilibrium, while mineral precipitation–dissolution kinetics are simulated using transition state theory rate laws (Aagaard and Helgeson, 1982). All reaction stoichiometry, equilibrium constants, and rate constants are included in the Supplementary Material (Tables S3–S5).

#### 3.4.2 Numerical experiments

To further examine inundation-driven solute flushing, we perform a series of numerical experiments that simulate multiple types and intensities of floods. All simulations begin with a spin-up period to initialize typical distributions of water, solutes, and minerals that occur following a full summer of evapotranspiration (ET). The 90-day spin-up period begins with a fully saturated soil column; initial aqueous concentrations within the soil represent average values from a nearby monitoring well (Table S6). Quartz, gypsum, and calcite are initially in equilibrium with porewater, using volume fractions derived from X-ray diffraction analyses (Looney et al., 2014). In contrast, the soil initially contains very little blödite (0.00001 $m^3\,m^{-3}$; Table S6).

https://doi.org/10.5194/egusphere-2026-4826
Preprint. Discussion started: 25 August 2026


**Table 1.** Overview of the flood scenarios tested during reactive transport simulations

| Scenario set | Inundation style | Flood duration (h) | Flood depth (cm) | Post-flood condition[a] |
|---|---|---|---|---|
| 1–12 | Top-down[b] | 48 | 2.72, 4.82, 10.0, 20.0, 30.0, 40.0 | Fall (no T) or spring (with T) |
| 13–24 | Bottom-up[c] | 3, 6, 12, 18, 24, 36 | 50.0 | Fall (no T) or spring (with T) |

[a]Each flood was followed by a 30-d simulation either without transpiration (fall flood) or with transpiration (spring flood), producing 24 total scenarios.
[b]Top-down floods were simulated by applying a specified discharge to the land surface, with total flood depth corresponding to the listed event depth.
[c]Bottom-up floods were simulated by applying a specified head at the base of the domain sufficient to raise the water table 0.5 m above the floodplain surface.

During the spin-up period, we apply a constant flux boundary condition at the surface equal to the average spring and summer precipitation rate (0.65 $\mathrm{mm\,d^{-1}}$) and a constant head boundary at the bottom of the domain equal to the typical water table elevation. Solute concentrations at the bottom boundary are equal to average observed concentrations in groundwater. Concentrations at the top boundary are reduced by two orders of magnitude relative to groundwater, which is designed to represent infiltration of dilute water from precipitation or surface runoff (Table S7). Throughout spin-up, water is gradually lost from the soil due to transpiration, which is parameterized using average reference ET observed at a nearby meteorological station and a crop coefficient for wheatgrass (0.82; Wight and Hanson, 1990). This transpiration drives upward flow of groundwater into the soil, evaporative concentration of porewater, and precipitation of evaporite minerals. Resultant water content and concentration profiles mimic those that occur in late summer prior to a fall flood. In years without significant fall precipitation, these profiles are also similar to those that occur in the early spring, assuming that wintertime ET and deep percolation are negligible.

Following the spin-up period, we simulate 12 different flood scenarios (Table 1), including both top-down and bottom-up inundation. To simulate bottom-up inundation, we apply a specified head of 2.0 m to the bottom of the domain, which drives the water table to 0.5 m above the surface; this configuration simulates a flood in which river stage rises 0.5 m above the floodplain elevation without breaching adjacent levees (Fig. 1b). Following the specified flood duration (Table 1), this boundary is reset to the pre-inundation value (a water table depth of 1.3 m). For top-down floods, we apply a specified discharge to the surface of the domain. The three smallest flood volumes in each top-down scenario (3, 5, and 10 cm; Table 1) correspond to the 95th percentile, 99th percentile and maximum single-storm precipitation totals observed at the site between 1924 and 2024. Larger top-down events (20, 30, and 40 cm) correspond to either river-driven flooding (Fig. 1d) or infiltration of melting snow. During top-down events, infiltrating water is partitioned between macropores and the soil matrix using the ratio of saturated hydraulic conductivity between the two domains (Lassabatere et al., 2014). At the end of each flood, the top boundary condition is reset to the long-term precipitation rate, as during spin-up.

In addition to varying the magnitude and style of inundation, we also vary inundation timing throughout the year by following each flood with 30-day simulations either with or without transpiration (Table 1). Simulations with post-flood transpiration mimic summer plant water demand following a spring flood. Because the Little Wind River floodplain often experiences intense storms in early fall, we include additional scenarios without transpiration to mimic fall conditions (plant senescence) following a September or October flood.

https://doi.org/10.5194/egusphere-2026-4826
Preprint. Discussion started: 25 August 2026


# 4 Results

## 4.1 Field observations

### 4.1.1 Top-down inundation

The soil dye test revealed extensive macropore flow along soil fractures, root channels, and worm burrows. Prior to the test, antecedent soil moisture in the upper 120 cm of soil ranged from 0.39 to 0.48 $m^3\,m^{-3}$, as measured from nearby time-domain reflectometers. The 55-cm ponding pulse took approximately 6.1 h to infiltrate into the soil, which equates to an average infiltration rate of 9.02 $cm\,h^{-1}$. Excavated horizontal soil sections (Fig. 3a–d) reveal that dyed water primarily percolated through the soil along macropores, with minimal flow through the soil matrix. In the shallow soil (0–30 cm), dominant macropores were soil cracks, while the middle of the profile (30–60 cm) included active and abandoned root channels and worm burrows.

While the volume of water applied at the surface was enough to fully saturate the upper 110–180 cm of the soil profile (assuming a porosity of 0.3 to 0.5), pockets of dry soil were observed from 20 cm depth down to the maximum depth of excavation (110 cm). Some pockets of dry soil contained intact evaporites immediately adjacent to dyed macropores (Fig. 3e), providing direct evidence that macropores allow flow to bypass the soil matrix.

### 4.1.2 Bottom-up inundation

While the dye tracer test simulated a top-down flood event, porewater sampling captured changes in water chemistry during a natural bottom-up flood. In June, mountain snowmelt drove a 1.4-meter increase in river stage over 7 d, before it peaked and gradually declined throughout the summer (Fig. S3). This rise in river stage was inadequate to breach the natural levees along the river channel, but still resulted in standing water along the floodplain, as it drove the water table from 1.25 m depth to 15 cm above the surface. Project personnel were in the field when the water table peaked and directly observed that the river did not spill over its banks.

The bottom-up flood induced rapid changes in soil porewater concentrations (Fig. 2). In the two months prior to the flood, concentrations of Na and Mg in soil porewater exhibited minimal temporal variability. Within 3 days following the peak in the water table, depth-averaged concentrations of Na and Mg increased 301% and 66%, respectively (Fig. 2). While similar patterns were observed across other elements, we only show results for Na and Mg as they are the cations found in blödite, the most abundant evaporite mineral at the site. Concentrations stayed elevated for approximately 3 weeks before decreasing slightly in early July and then remaining elevated for the remainder of the summer with a gradual decrease in the fall.

Multiple mechanisms could have contributed to this sudden increase in solute concentrations. First, within the shallow soil, dissolution of evaporite minerals such as blödite would raise Na and Mg concentrations. Second, wetting up of the soil matrix may have mobilized stagnant, solute-rich water that was previously trapped in disconnected pores and inaccessible to the porewater samplers. Third, due to the history of uranium ore processing at the Little Wind River site, groundwater in the alluvial aquifer is enriched in Na, Mg, Ca, Cl, sulfate, and other ions relative to the soil (Dam et al., 2015; U.S. Department of Energy, 2016). Thus, the bottom-up flood could have driven upward advection of solute-rich groundwater, contributing to the

https://doi.org/10.5194/egusphere-2026-4826
Preprint. Discussion started: 25 August 2026


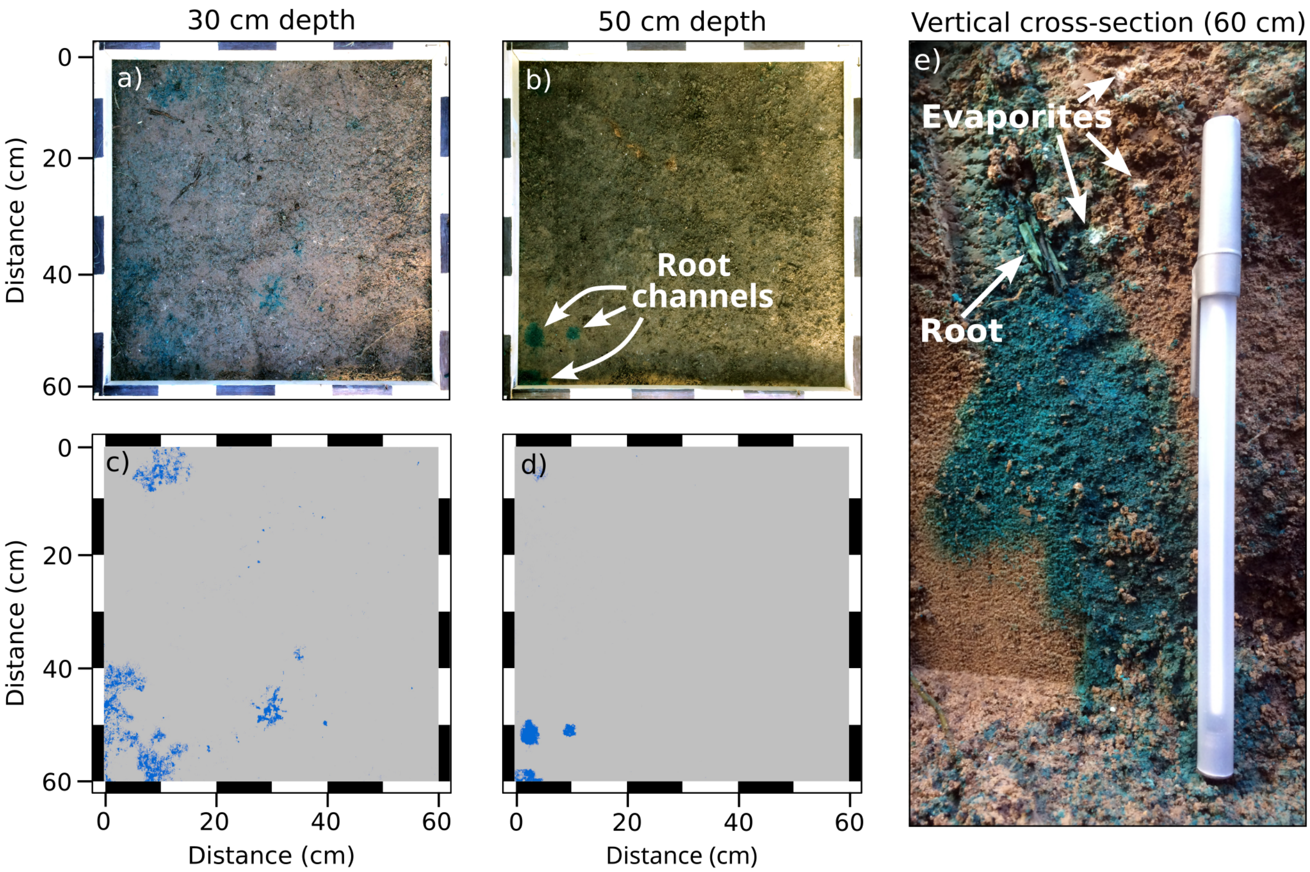


**Figure 3.** Orthorectified photographs (a, b) of two horizontal cross-sections from the dye infiltration test, along with corresponding images (c, d) classified into dye-stained and unstained areas. A close-up image from a vertical cross-section at 60 cm depth (e) shows that dye-stained water flowed along a root channel, adjacent to dry soil with intact evaporites.

observed concentration increase within the soil. Together, these mechanisms indicate that bottom-up inundation mobilized solutes both within the soil profile and from the underlying aquifer.

### 4.2 Reactive transport simulations

While field data captured solute flushing dynamics during one top-down and one bottom-up inundation event, reactive transport simulations allow us to explore these processes under a wider range of conditions. Because model simulations were not designed to replicate field observations, we do not perform any direct comparison to field measurements. Nonetheless, simulations exhibit similar solute transport dynamics as observed in the field.

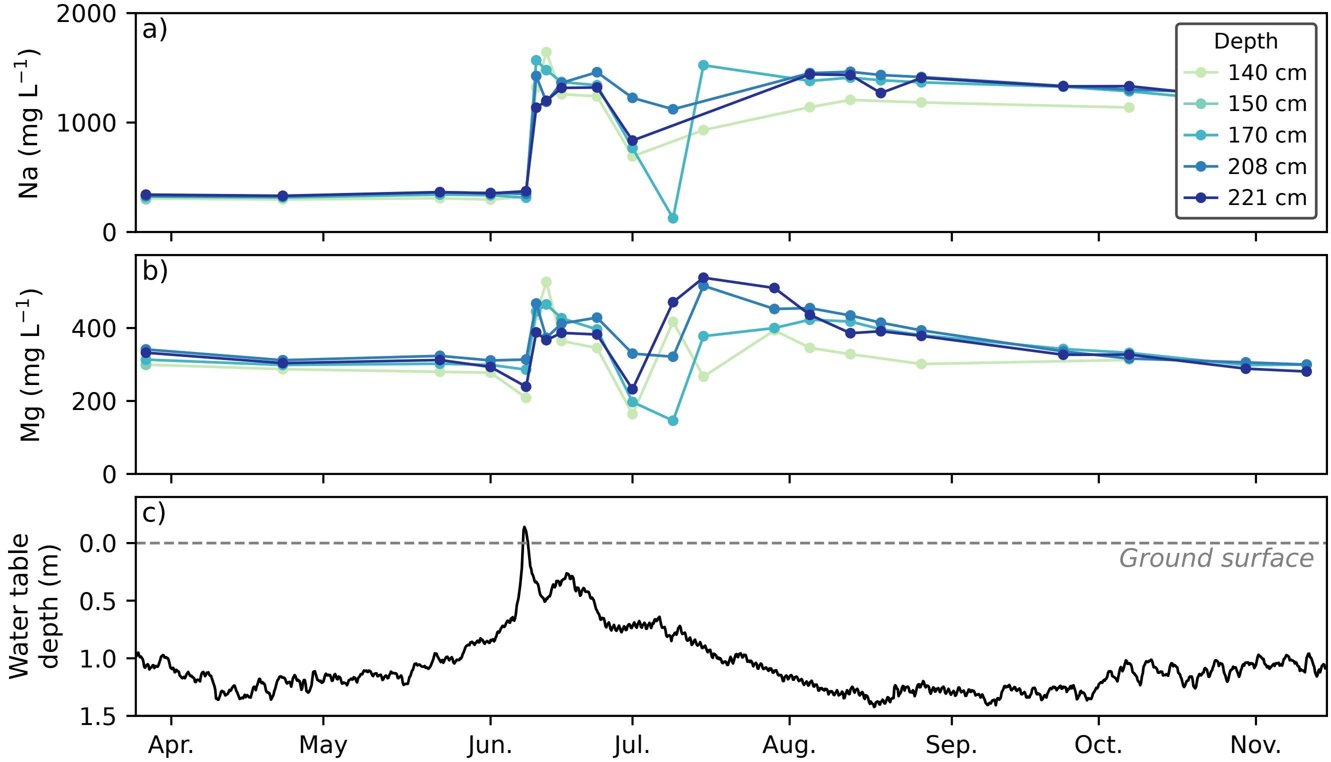


**Figure 4.** Observed porewater concentrations of Na (a) and Mg (b), along with water table depth (c) from a nearby monitoring well. A bottom-up flood in June coincided with a sudden increase in porewater concentrations of several elements. Porewater samples are colored by depth and correspond to the same colors as in Fig. 2.

#### 4.2.1 Simulation spin up

The spin-up period initialized soil water content, mineral, and solute profiles (Fig. 5) that are largely similar to those observed in the field prior to inundation. At the start of spin up, the soil matrix is fully saturated (Fig. 5a) and root water uptake decreases exponentially with depth (Fig. 5b) as a result of the prescribed root distribution (Jackson et al., 1996). Within 10 days, water content in the shallow soil decreases rapidly under gravity drainage with a concurrent decrease in root water uptake (Fig. 5b). Beyond 10 days, water content in the soil matrix and root water uptake both reach a quasi steady state. During this time, minimal root water uptake occurs from 15–40 cm depth because soil moisture drops below the wilting point (Fig. 5b). At deeper depths, transpiration is mostly sustained by upward flow from the underlying aquifer (Fig. S4) In contrast, hotspots of evapotranspiration (ET) occur at the surface (supported by the inflow of water from precipitation) and at 40–60 cm depth (the shallowest point at which root water uptake is not limited by soil moisture).

These hotspots of ET lead to the concentration of soil porewater (Fig. 5) through evapoconcentration and solute exclusion during transpiration. Though subsequent discussion primarily focuses on $Mg^{2+}$, results are similar for other solutes. As solute

https://doi.org/10.5194/egusphere-2026-4826
Preprint. Discussion started: 25 August 2026


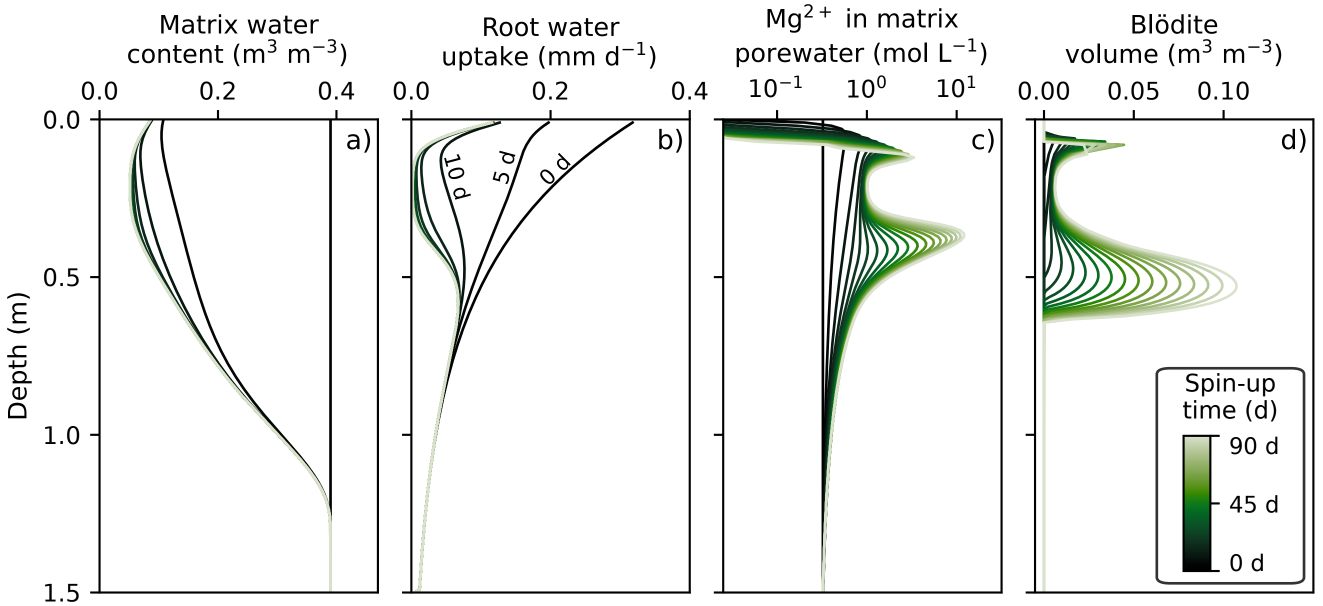


**Figure 5.** Changes in soil matrix water content, root water uptake, $Mg^{2+}$ in matrix porewater, and blödite volume (the most reactive evaporite mineral) during the spin-up period. Lines are plotted every 5 d. Profiles for other solutes and other minerals are shown in the Supplementary Material.

concentrations increase, evaporites form at 50 cm depth, which agrees with field observations (Fig. 2). Most of the change in evaporite volume comes from blödite precipitation, while volume fractions of other minerals remain constant (Fig. S5). Because blödite is the most abundant evaporite mineral at this field site and the most reactive mineral in these simulations, subsequent analyses focus primarily on blödite, though results are expected to hold for other soluble evaporites, such as halite, sylvite, hexahydrite, and thenardite.

#### 4.2.2 Top-down inundation

During each top-down inundation event, the majority of floodwater (mean 73%) infiltrates into soil macropores, while the wetting front propagates more slowly through the soil matrix. Changes in water content, $Mg^{2+}$ concentrations, and blödite volume for a 20-cm top-down flood are shown in Fig. 6a–d, though equivalent plots for other top-down floods are included in the Supplementary Material (Fig. S6). Even in the most intense inundation event (40 cm over 2 d), the soil wetting front only propagates to 45 cm depth in the soil matrix even though it quickly saturates soil macropores. Tracers added to the inundation water emphasize this dichotomy; while tracers rapidly move through macropores, they only propagate to 30 cm depth within the soil matrix (Fig. S7). Because the wetting front does not propagate very deeply into the soil matrix, the simulations exhibit minimal dilution of soil solutes, such as $Mg^{2+}$, and minimal evaporite dissolution (Fig. 6d and Fig. S6). Across all top-down flood scenarios, the fraction of blödite dissolved during inundation ranges from 4.2 to 18.8%.

https://doi.org/10.5194/egusphere-2026-4826
Preprint. Discussion started: 25 August 2026


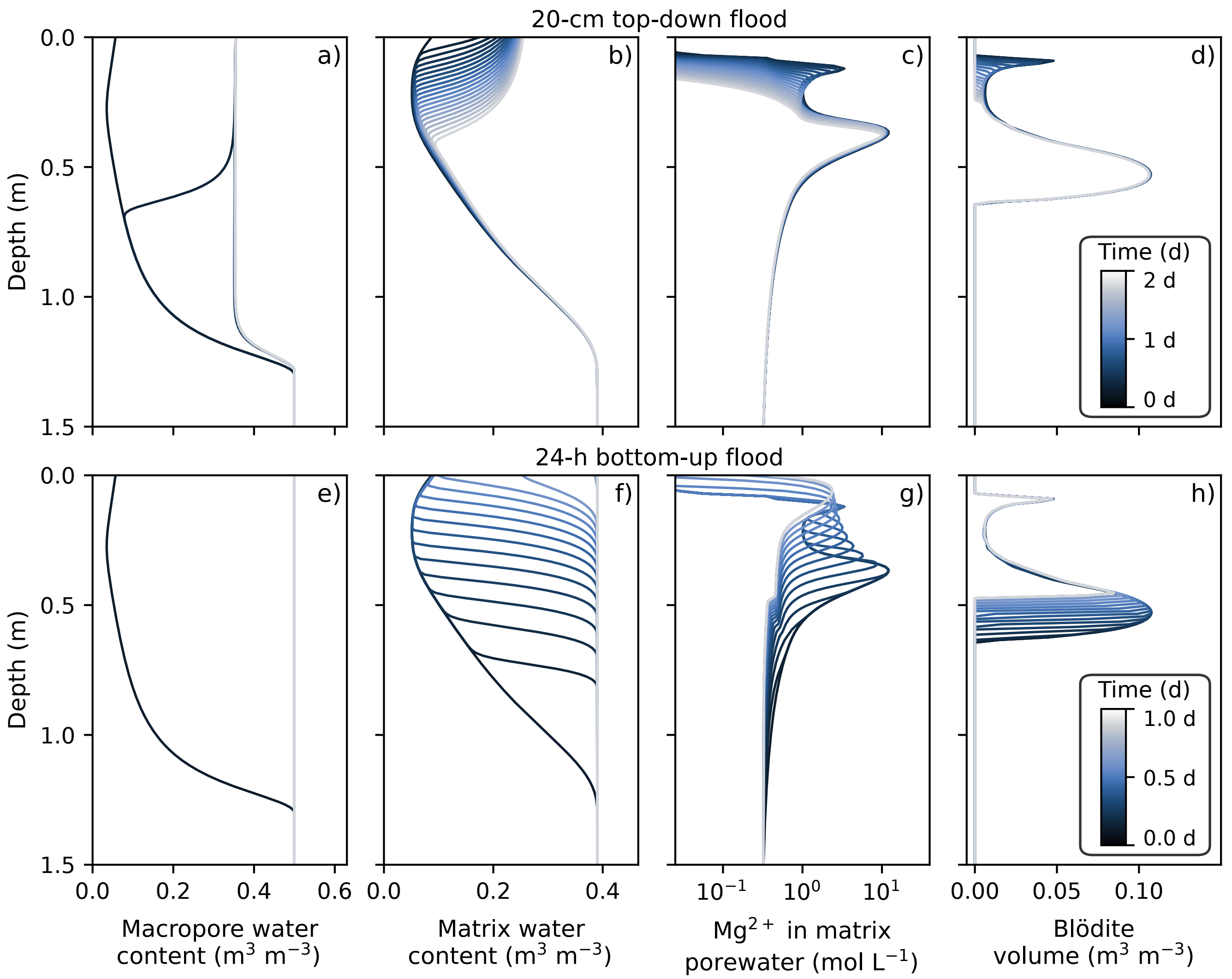


**Figure 6.** A comparison of changes in macropore water content (a, e), soil matrix water content (b, f), $Mg^{2+}$ concentrations in matrix porewater (c, g), and blödite volume (d, h) during a 20-cm, top-down flood (a–d) and a 24-h, bottom-up flood (e–h). During the top-down flood, water predominantly flowed through soil macropores, resulting in minimal blödite dissolution, while the bottom-up flood saturated both the macropores and soil matrix, dissolving evaporites such as blödite. Lines are plotted every 0.1 d in (a)–(d) and every 0.05 d in (e)–(h).

### 4.2.3 Bottom-up inundation

During each bottom-up flood, the soil macropores saturate almost immediately, while the soil matrix gradually wets up from below (Fig. 6e-f and Fig. S8). While the simulated inundation depth was the same across each scenario (0.5 m above the land surface), flood duration exerts an important control on the upward propagation of the wetting front (Fig. S8); the water table takes approximately 12 h to rise above the land surface, so floods shorter than 12 h do not fully saturate the soil matrix.

Tracer profiles show that groundwater from the underlying aquifer flows up into the soil, reaching up to 70 cm depth (Fig. S7). This upward flow of groundwater displaces soil porewater, resulting in an upward shift in peak $Mg^{2+}$ and other solute concentrations (Fig. 6g and Fig. S8). This upward flow also drives a net inflow of solutes from the aquifer to the soil (Fig. S9), since any upward-flowing groundwater carries dissolved solutes across the soil–aquifer interface.

While minimal evaporite dissolution occurred during top-down inundation, bottom-up floods dissolve much of the blödite present in the soil profile. Across all scenarios, the fraction of blödite dissolved during bottom-up inundation ranges 4.1–58.3%, while less soluble minerals, such as quartz, calcite, and gypsum, exhibit minimal change in volume fraction. Given that mineral dissolution is often kinetically limited, flood duration exerts an important control on mineral dissolution, with longer events leading to more blödite dissolution (Fig. S8).

#### 4.2.4 Seasonal timing of inundation

The hydrologic forcing following inundation exerts another important control on solute exchange between the soil and the underlying aquifer. Each inundation event in Table 1 was followed by 30 days either with or without transpiration, mimicking summer conditions (during the growing season) following a spring flood and late fall conditions (post plant senescence) following a fall flood, respectively. Figure 7 compares the impact of post-flood transpiration on soil moisture and solute concentrations following the 24-hour bottom-up flood shown in Fig. 6e–h. In both scenarios, the soil macropores drain rapidly as the water table recedes (Fig. 7a, e). Water content in the soil matrix declines rapidly as well, though the decrease occurs faster in simulations with transpiration (Fig. 7b, f). Following the spring flood, solute concentrations steadily increase through evaporative concentration and solute exclusion during root water uptake (Fig. 7c). In contrast, following the fall flood, peak $Mg^{2+}$ concentrations steadily move down in the soil profile as a result of steady recharge from the surface (Fig. 7g). Though the spring flood also receives this steady recharge at the surface ($0.65\ \mathrm{mm\,d^{-1}}$), it is outweighed by transpiration, which results in almost no downward migration of soil solutes.

Following the spring flood, increasing $Na^{+}$, $Mg^{2+}$, and $SO_4^{2-}$ concentrations lead to renewed blödite precipitation in the soil profile (Fig. 7d). In contrast, the lack of transpiration following the fall flood allows rainfall to percolate down through the soil matrix, resulting in blödite dissolution (Fig. 7h). Total blödite volume increases 278% in the 30 days following the spring flood, whereas total blödite volume decreases by 20% in the 30 days following the fall flood. This pattern is consistent across the full suite of flood scenarios (Fig. 8). While top-down floods exhibit minimal short-term evaporite dissolution (Fig. 8a), bottom-up floods initially produce blödite losses, reflecting the greater degree of matrix wetting and longer residence times allowing for dissolution during bottom-up inundation (Fig. 8b).

However, the persistence of these changes depends on post-flood conditions. In simulations without transpiration, both top-down and bottom-up inundation events result in net blödite loss due to steady recharge from the surface, percolation of solute-depleted rainfall, and continued evaporite dissolution (Fig. 8). In simulations with transpiration, this pattern reverses: root water uptake outweighs steady recharge of rainfall and promotes renewed blödite precipitation. As a result, all blödite lost during inundation is recovered, and total blödite volume increases above pre-flood values. This effect is strongest following bottom-up floods, which result in a net gain in blödite volume of 43–55% relative to pre-flood conditions, compared to 26–39% following

https://doi.org/10.5194/egusphere-2026-4826
Preprint. Discussion started: 25 August 2026


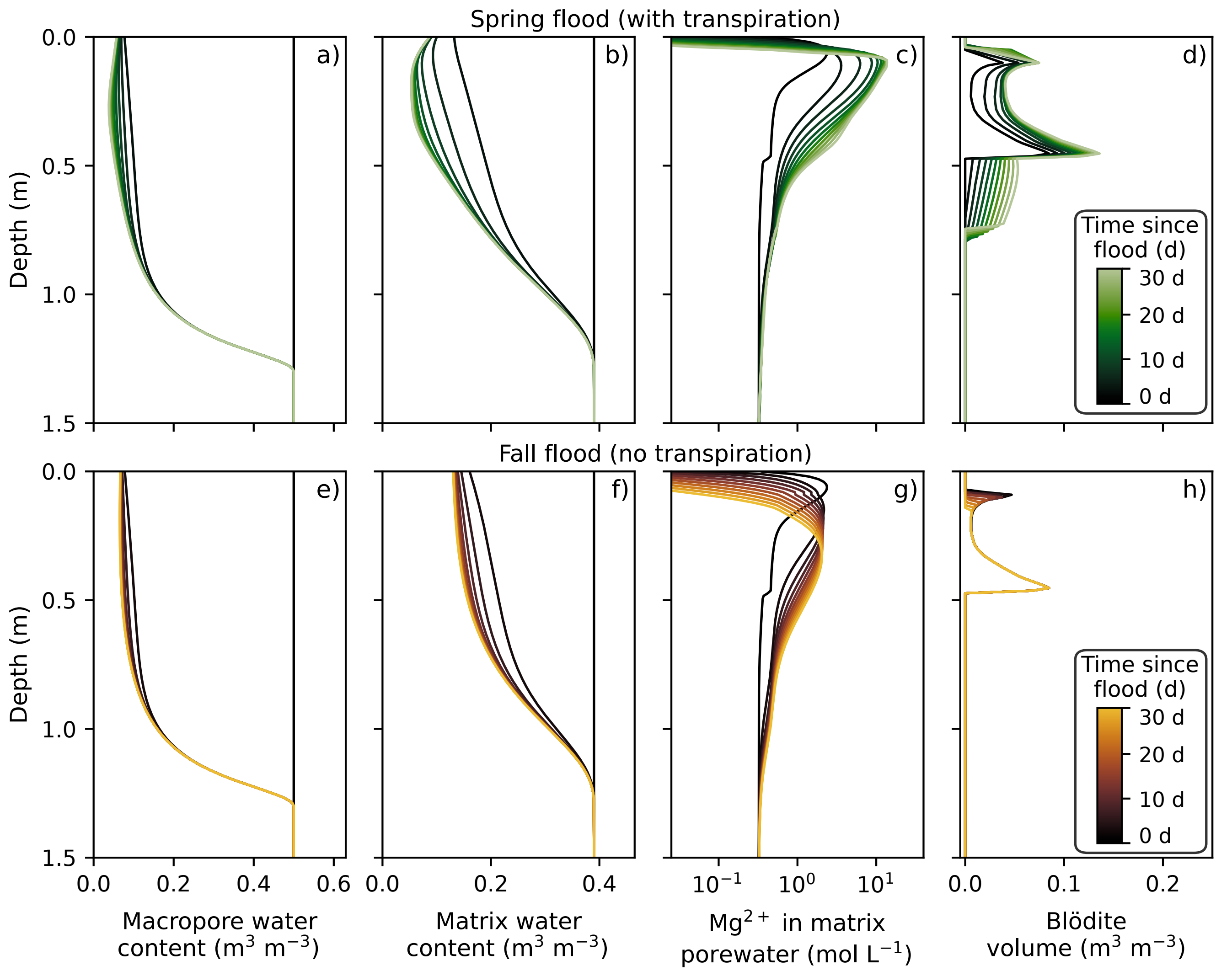


**Figure 7.** Changes in macropore water content, soil matrix water content, $Mg^{2+}$ in matrix porewater, and blödite volume (the most reactive evaporite mineral) following a spring bottom-up flood (a–d) and a fall bottom-up flood (e–h). Both simulations follow the 24-h, bottom-up flood shown in Fig. 6e–h. Lines are plotted every 5 d.

top-down floods (Fig. 8). This larger gain occurs because bottom-up inundation transports additional solutes and water into the soil profile, which in turn support greater transpiration, concentration of soil porewater, and evaporite precipitation. These results highlight that post-flood conditions can overshadow the immediate impact of mineral dissolution during inundation.

https://doi.org/10.5194/egusphere-2026-4826
Preprint. Discussion started: 25 August 2026


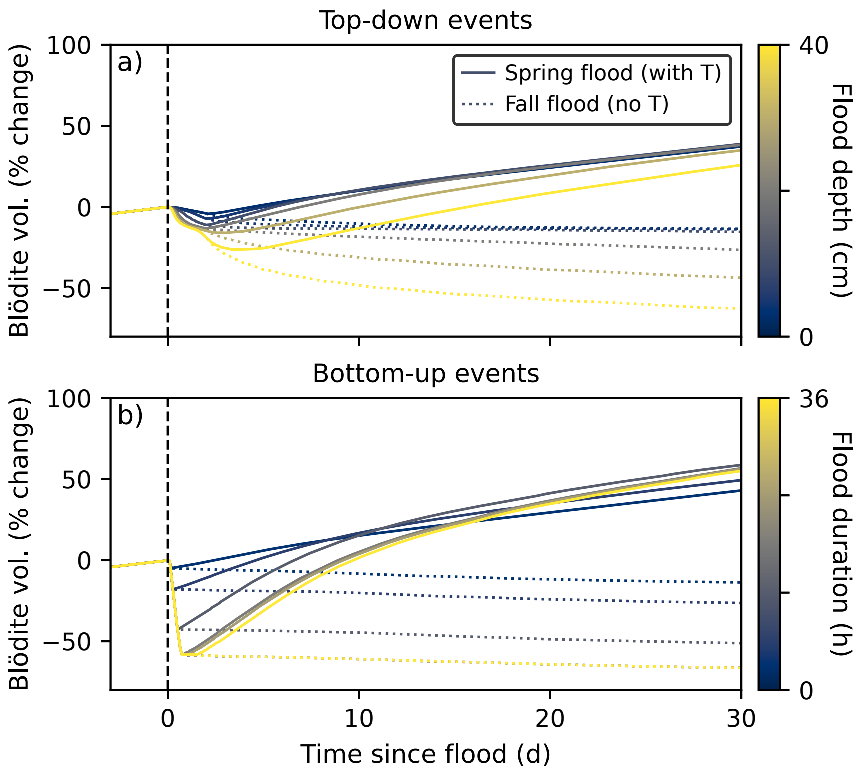


**Figure 8.** Time series of the change in blödite volume (the least soluble evaporite mineral) across all top-down (a) and bottom-up (b) flood scenarios. Solid lines indicate spring floods followed by summer transpiration (T), while dotted lines indicate fall floods followed by a winter period with no transpiration.

### 4.3 Net solute exchange between soil and aquifer

To evaluate whether these profile-scale changes result in net solute export or retention, we calculated the net solute exchange between the soil and underlying aquifer (Fig. 9 and Fig. S10–S11), using a control plane at 1.3 m depth to represent the position of the water table at baseflow. Although we show results for a subset of solutes ($Mg^{2+}$, $Na^{+}$, $SiO_2$ (aq), $Cl^{-}$, and an inert tracer), similar trends occur for other major ions.

While all top-down floods resulted in short-term solute flushing, only fall top-down floods led to sustainable solute losses to the aquifer (Fig. 9). In these simulations, the lack of transpiration allowed the pulse of floodwater to slowly percolate through the soil matrix and flush accumulated solutes (Fig. S12), driving long-term losses to the aquifer (Fig. 9). For floods followed by transpiration, the pulse of floodwater is rapidly taken up by plant roots, which counteracts downward percolation and solute export. As a result, these simulations exhibit net solute gains from the aquifer to the soil.

Bottom-up floods, on the other hand, initially transported groundwater solutes upward into the soil profile as a result of the upward flow from below (Fig. 9). By 30 days after the flood, the magnitude of this gain depends strongly on transpiration, which helps to retain solutes in the soil. Following spring floods, for example, 71–100% of the $Mg^{2+}$ delivered during inundation was retained in the soil due to summer transpiration. By comparison, only 9–74% of this $Mg^{2+}$ was retained following fall floods. Together, these results demonstrate that flood direction controls the initial extent and direction of solute exchange, while post-flood transpiration determines whether mobilized solutes are ultimately exported to the aquifer or retained in the soil.

## 5 Discussion

### 5.1 Bottom-up and top-down floods produce distinct export signals

Floodplain inundation is often conceptualized as a flushing process, in which water entering the floodplain mobilizes accumulated solutes and transports them toward aquifers and surface water. However, our results indicate that inundation does not induce uniform flushing of soil porewater. Instead, solute transport depends on the type of inundation event (bottom-up vs top-down), the flowpaths that floodwater takes through the soil, and the post-flood water balance. Top-down floods rapidly infiltrate via preferential flow and percolate through the vadose zone along macropores. This flow bypasses the soil matrix, resulting in minimal solute losses from the soil to the aquifer. Because preferential flow occurs in nearly all soils (Beven and Germann, 1982; Jarvis, 2007; Orozco-López et al., 2018; Nimmo, 2021), this process likely dominates during top-down inundation of many floodplains, not just the Little Wind River floodplain. However, this form of preferential flow primarily occurs under unsaturated conditions; thus, its impact will depend on the elevation of the water table prior to inundation.

In contrast, bottom-up inundation wets up the soil matrix from below, dissolves soluble minerals, and drives solutes from the underlying aquifer up into the soil. This process explains the rapid increase in Na and Mg concentrations observed in field samples following the bottom-up flood (Fig. 2); the rising water table saturated the soil matrix and dissolved evaporite minerals, increasing porewater concentrations. Across both field observations and model simulations, bottom-up floods produce an immediate net gain of solutes to the soil, rather than flushing solutes downward to the aquifer. Although our analysis focuses primarily on $Mg^{2+}$ and blödite, similar trends for other aqueous species and inert tracers (Fig. 9) suggest that these processes apply more broadly to any solutes that accumulate in soil porewater.

### 5.2 Post-flood conditions control net solute exchange

While the type of inundation event controls solute exchange in the short term, field and modeling results indicate that the post-flood water balance determines whether inundation leads to sustained solute export. When spring floods are followed by summer evapotranspiration, root water uptake counteracts downward transport due to gravity. As plants dewater the soil, water-filled pores become disconnected. Evaporation and root solute exclusion then promote porewater concentration and subsequent evaporite precipitation. These results help explain why soil porewater concentrations on the Little Wind River floodplain remained elevated throughout the summer following the spring flood, as transpiration limited downward percolation of soil porewater (Fig. 2).

https://doi.org/10.5194/egusphere-2026-4826
Preprint. Discussion started: 25 August 2026


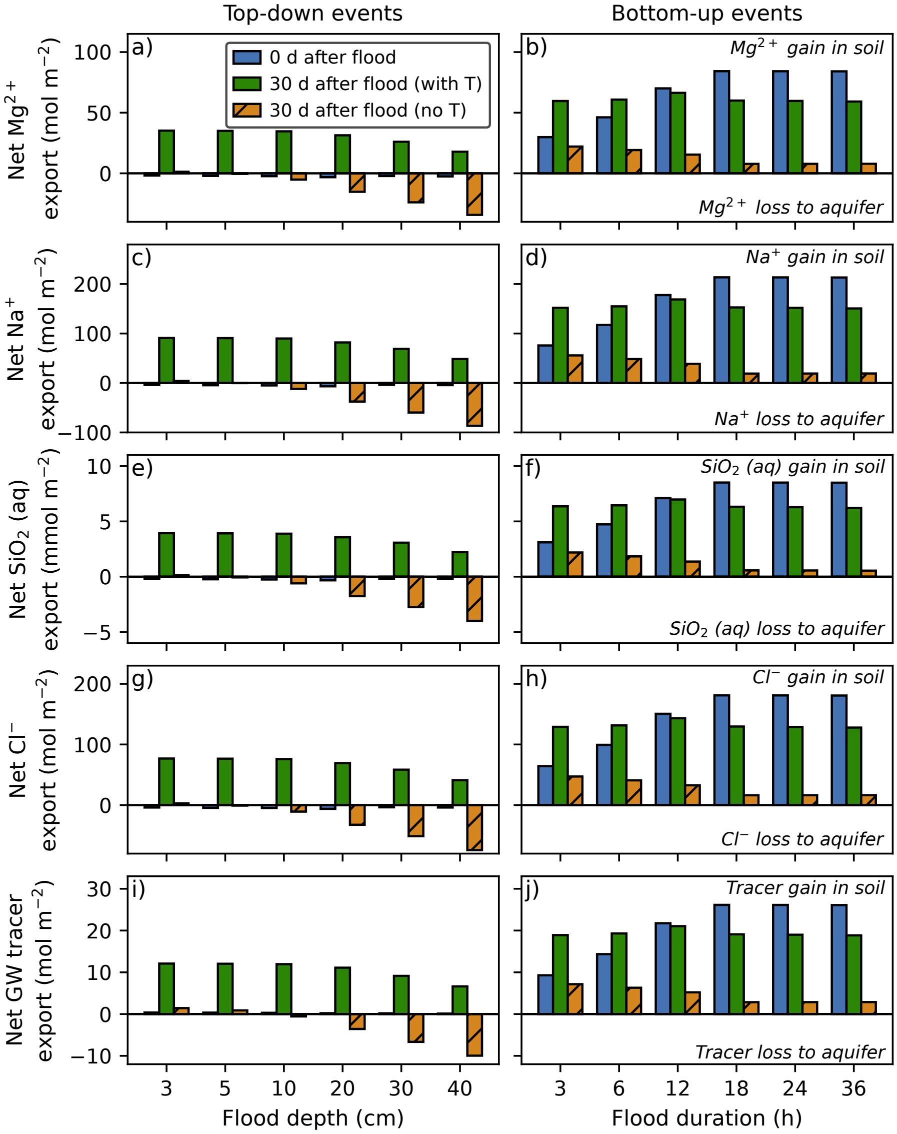


**Figure 9.** Net gain or loss of several solutes from the soil to the underlying aquifer for both top-down and bottom-up flood scenarios with and without transpiration (T). Cumulative solute loss is shown immediately after each flood (blue bars), after 30 d of transpiration (green bars), and after 30 d without transpiration (orange hashed bars). Net solute exchange was calculated across a control plane at 1.3 m depth, and negative values represent net solute losses from the soil to the aquifer. Note that the groundwater tracer (i, j) is an inert tracer with low initial concentrations in the soil (0.001 $\mathrm{mol\,L^{-1}}$) and high concentrations in the underlying aquifer (0.1 $\mathrm{mol\,L^{-1}}$).

In reactive transport simulations, 30 days of summer evapotranspiration was enough to outweigh even the most intense spring floods, preventing floodwater from reaching the saturated zone and trapping solutes in the soil (Fig. 9 and S12). This observation highlights the difficulty of flushing solutes from arid and semi-arid floodplains, which can lead to long-term salinization (Jolly

https://doi.org/10.5194/egusphere-2026-4826
Preprint. Discussion started: 25 August 2026


et al., 1993; Crosbie et al., 2009). These results also suggest a potential link between altered flood regimes and long-term floodplain salinity. If changes in climate or river management reduce the occurrence of floods capable of flushing floodplain soils, repeated inundation followed by intense summer evapotranspiration could redistribute salts within the soil profile without exporting them, promoting progressive salinization.

Despite these barriers to solute leaching, slow and steady infiltration of precipitation can promote downward long-term solute flushing. Macropore flow is most often activated when water ponds on the surface and flows into soil macropores (Jarvis, 2007). Thus, diffuse recharge from low-intensity precipitation primarily infiltrates into the soil matrix, leading to downward percolation and flushing of matrix porewater. Simulations of fall floods reinforce this process; when transpiration is turned off, steady recharge from the surface promotes downward percolation of rainwater, continued evaporite dissolution, and net solute loss from the soil to the aquifer (Fig. 9). Under these conditions, steady recharge mitigates the initial solute gain that occurs during bottom-up floods. The contrasting results between spring and fall floods highlight the importance of seasonal timing on net solute exchange: fall floods favor solute flushing, whereas spring floods favor solute retention and re-accumulation.

### 5.3 Broader implications for floodplain function

Our results have implications beyond floodplain biogeochemistry. Concentration–discharge (C–Q) relationships provide a widely used framework for understanding how inundation activates distinct flowpaths and solute sources within a watershed. While riverine C–Q patterns integrate solute production and transmission across the entire watershed, floodplains can strongly influence those patterns in reaches with substantial river–aquifer exchange (Sawyer et al., 2014; Rose et al., 2018).

Although many rivers display stable C-Q relationships over time, some exhibit event-specific C-Q behavior, switching from a dilution pattern during one flood to enrichment in another (e.g., Chanat et al., 2002; Knapp et al., 2020). Our results provide one mechanistic explanation for this event-to-event variability. For example, a top-down flood may generate rapid preferential flow without flushing solutes from the soil matrix, contributing to dilution in the C–Q signal (Fig. 10). A bottom-up flood, on the other hand, could produce the same inundation depth at the land surface, but lead to enrichment patterns driven by greater interactions with the soil matrix and mobilization of stored solutes. Thus, inundation extent or discharge response cannot in isolation predict the direction or magnitude of floodplain solute export; instead, solute mobilization depends on whether the event connects moving water to reactive storage zones.

Our results also illustrate how preferential flow can contribute to hysteresis in the C–Q signal. Hysteresis typically occurs when concentration differs between the rising and falling limbs of a flood, reflecting a temporal offset between the hydraulic response and the mobilization of solutes (Evans and Davies, 1998; House and Warwick, 1998; Bieroza and Heathwaite, 2015; Arora et al., 2020). This behavior is evident in the simulated concentration and discharge response at the soil–aquifer interface during a 40-cm top-down flood (Fig. 10). Initially, the flood generates rapid flow along macropores with limited flushing of solutes from the soil matrix, corresponding to dilution during the rising limb of the C–Q signal. Later, solute-rich water draining from the soil matrix reaches the aquifer, causing concentrations to rise after discharge has already peaked (Fig. 10 and S12e-h). Although these C–Q patterns are quantified at the soil–aquifer interface rather than within the river channel, they demonstrate

https://doi.org/10.5194/egusphere-2026-4826
Preprint. Discussion started: 25 August 2026


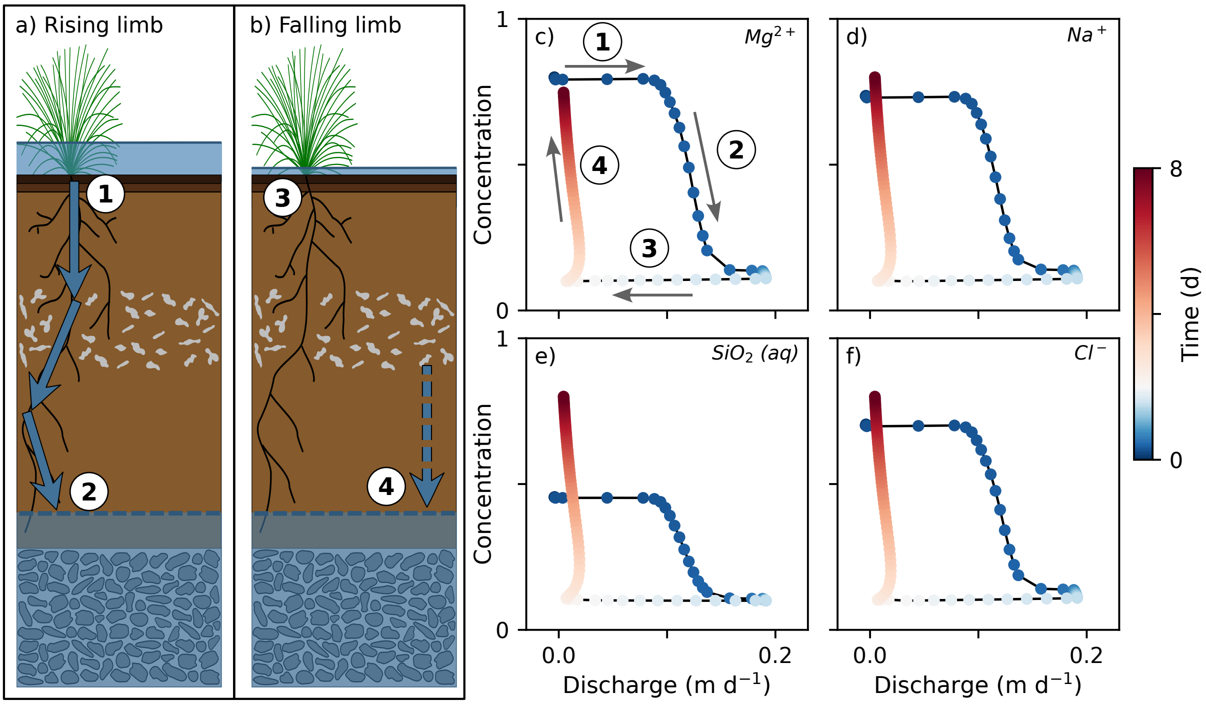


**Figure 10.** Illustration of the flowpaths activated during a top-down flood (a, b) and the changes in concentration and discharge of several solutes during simulations of a 40-cm, top-down flood (c–f). Initially, water infiltrates along macropores (1), causing an increase in discharge without corresponding changes in concentration. When floodwater reaches the soil–aquifer interface (2), it dilutes pre-event water, causing a decrease in concentration. During the falling limb, discharge decreases as water no longer preferentially flows into macropores (3). Then, several days after the flood, concentrations increase again due to the delayed arrival of solute-rich water from the soil matrix (4). Note that both concentration and discharge are measured at the soil–aquifer interface and concentration is normalized between 0 and 1 for comparison across solutes. The simulation includes 2 d of inundation (blue points) followed by a recession period without evapotranspiration forcing (red points).

a floodplain-scale mechanism that could contribute to reach-scale hysteresis. Moreover, these results show how a floodplain can shift from transmitting dilute water to exporting stored solutes over the course of a single event.

More broadly, these results suggest that floodplain function cannot be inferred from flood frequency or duration alone. Ecohydrology studies, for example, have shown that inundation exerts a dominant control on floodplain vegetation growth (Blom and Voesenek, 1996). While early work focused primarily on flood extent, more recent research has shown that vegetation patterns are also impacted by the source of inundation water (Berezowski and Wassen, 2023). Our results provide a complementary biogeochemical mechanism to explain this pattern; riparian vegetation growth is strongly impacted by soil water chemistry (Ellery et al., 1993; Dosskey et al., 2010), and our simulations show that different forms of inundation produce distinct soil solute responses. This research also has implications for nutrient management, floodplain restoration, and contaminant mobilization research. Floodplain restoration projects often aim to increase hydrologic connectivity by increasing

https://doi.org/10.5194/egusphere-2026-4826
Preprint. Discussion started: 25 August 2026


inundation frequency (Newcomer Johnson et al., 2016; McMillan and Noe, 2017), but our results imply that not all types of inundation result in solute flushing, nutrient delivery, or contaminant export. Instead, the biogeochemical outcome depends on the source of inundation water and the degree of contact with reactive storage zones.

### 5.4 Limitations and future work

We acknowledge several limitations of our approach. First, field observations captured only one top-down and one bottom-up inundation event, limiting our ability to evaluate a broad range of flood intensities under field conditions. As discussed in Section 2, some floods may result from a combination of top-down and bottom-up mechanisms. We were unable to study these mixed inundation events under field conditions and they may result in different solute transport signals than were captured by either end member. Second, reactive transport simulations were designed to explore fundamental processes rather than reproduce field observations. To support model interpretability, we developed parsimonious simulations with simplified soil structure, macropore–matrix exchange terms, vegetation dynamics, and mineral phases. Future work could incorporate additional complexities into model simulations — such as a heterogeneous soil profile or a more extensive reaction network — and evaluate their impact on solute dynamics. Despite these limitations, our combined field and modeling results suggest that the driver of inundation, the extent of preferential flow, and the post-flood water balance exert first-order controls on solute flushing or retention in floodplain soils.

## 6 Conclusions

This paper examines the impact of distinct types of inundation events (Fig. 1) on solute export from floodplain soils. While floodplain inundation is often assumed to flush solutes out of the soil profile, our results highlight that this response is not universal. Instead, solute mobilization depends on the mechanism of inundation, the flowpaths activated during flooding, and the post-flood water balance. We conclude that:

1. Top-down and bottom-up inundation produce fundamentally different soil wetting patterns. During top-down inundation, floodwater rapidly infiltrates through macropores and bypasses much of the soil matrix, limiting contact with stored solutes and evaporite minerals. During bottom-up inundation, groundwater rises into the soil profile and wets up the profile from below, fully saturating both the soil matrix and the macropores.

2. Preferential flow can increase hydrologic connectivity without driving solute flushing. In the dye tracer test and simulations, large volumes of surface-applied water moved rapidly through macropores while leaving portions of the soil matrix relatively dry. As a result, top-down floods can produce rapid water movement through the profile without appreciable solute exchange.

3. The type of inundation event controls the direction of solute exchange between the soil and aquifer. Top-down floods initially drive solute losses from the soil toward the aquifer, although these losses are small when flow bypasses the

matrix. In contrast, bottom-up floods initially transport groundwater solutes upward into the soil profile, producing a net solute gain to the soil rather than immediate flushing to the aquifer.

4. The seasonal timing of inundation determines whether mobilized solutes are exported or retained. When spring floods are followed by intense plant water demand, root water uptake counteracts downward percolation, concentrates soil porewater, and promotes evaporite precipitation. In contrast, when floods occur after plant senescence, diffuse recharge through the soil matrix promotes steady downward flow and solute export. These results demonstrate that interpreting floodplain solute dynamics requires distinguishing not only the magnitude of inundation, but also its source, flowpath, and seasonal timing.

*Code and data availability.* All simulations were performed with the MIN3P-DP branch of the MIN3P reactive transport code (https://github.com/min3p-ubc/min3p). Model input files, selected raw model output, and processed model output will be available to the public via a Zenodo repository.

*Author contributions.* ZP, KB, KM, and JB designed the field experiments while ZP carried out the field investigation and collected samples. ZP developed model simulations and conducted the formal analyses. KB, KM, and JB supervised the project and acquired funding. ZP prepared the original manuscript and figures, with review and editing contributions from all co-authors.

*Competing interests.* The authors declare no competing interests.

*Acknowledgements.* We would like to thank the Northern Arapaho Tribe for field access and support, especially Ryan Ortiz, Dean Googles, and Steve Babits of the Northern Arapaho Natural Resources Office. In addition, we thank St. Stephens Indian Mission, the local landowner, for permitting research on their land. We also thank Jacki Klancher, Cassie Weed, and Bailey Lewis of Central Wyoming College for their assistance with field sampling.

https://doi.org/10.5194/egusphere-2026-4826
Preprint. Discussion started: 25 August 2026


## References

Aagaard, P. and Helgeson, H.: Thermodynamic and kinetic constraints on reaction rates among minerals and aqueous solutions; I, Theoretical considerations, American Journal of Science, 282, 237–285, https://doi.org/10.2475/ajs.282.3.237, 1982.

Abboud, J., Ryan, M., and Osborn, G.: Groundwater flooding in a river-connected alluvial aquifer, Journal of Flood Risk Management, 11, e12 334, https://doi.org/10.1111/jfr3.12334, 2018.

Allgeier, J., Martin, S., and Cirpka, O.: Systematic Evaluation of Geometry-Driven Lateral River-Groundwater Exchange in Floodplains, Water Resources Research, 57, e2021WR030 239, https://doi.org/10.1029/2021WR030239, 2021.

Amoros, C. and Bornette, G.: Connectivity and biocomplexity in waterbodies of riverine floodplains, Freshwater Biology, 47, 761–776, https://doi.org/10.1046/j.1365-2427.2002.00905.x, 2002.

Arora, B., Burrus, M., Newcomer, M., Steefel, C. I., Carroll, R. W. H., Dwivedi, D., Dong, W., Williams, K. H., and Hubbard, S. S.: Differential C–Q Analysis: A New Approach to Inferring Lateral Transport and Hydrologic Transients Within Multiple Reaches of a Mountainous Headwater Catchment, Frontiers in Water, 2, 24, https://doi.org/10.3389/frwa.2020.00024, 2020.

Babey, T., Boye, K., Tolar, B., Engel, M., Noël, V., Perzan, Z., Kumar, N., Francis, C. A., Bargar, J. R., and Maher, K.: Simulation of anoxic lenses as exporters of reactivity in alluvial aquifer sediments, Geochimica et Cosmochimica Acta, 334, 119–134, https://doi.org/10.1016/j.gca.2022.07.018, 2022.

Babey, T., Perzan, Z., Pierce, S., Rogers, B., Wang, L., Carroll, R. W. H., Bargar, J. R., Boye, K., and Maher, K.: Mountainous Floodplain Connectivity in Response to Hydrological Transitions, Water Resources Research, 60, e2024WR037 162, https://doi.org/10.1029/2024WR037162, 2024.

Bates, P. D., Stewart, M. D., Desitter, A., Anderson, M. G., Renaud, J., and Smith, J. A.: Numerical simulation of floodplain hydrology, Water Resources Research, 36, 2517–2529, https://doi.org/10.1029/2000WR900102, 2000.

Battaglia, M. and Sands, P. J.: Modelling Site Productivity of Eucalyptus globulus in Response to Climatic and Site Factors, Australian Journal of Plant Physiology, 24, 831–850, https://doi.org/10.1071/PP97065, 1997.

Bayley, P.: Understanding large river-floodplain ecosystems, BioScience, 45, 153–158, https://doi.org/10.2307/1312554, 1995.

Berezowski, T. and Wassen, M.: Using water sources extent during inundation as a reliable predictor for vegetation zonation in a natural wetland floodplain, Ecological Indicators, 154, 110 854, https://doi.org/10.1016/j.ecolind.2023.110854, 2023.

Bernhardt, E. S., Blaszczak, J. R., Ficken, C. D., Fork, M. L., Kaiser, K. E., and Seybold, E. C.: Control Points in Ecosystems: Moving Beyond the Hot Spot Hot Moment Concept, Ecosystems, 20, 665–682, https://doi.org/10.1007/s10021-016-0103-y, 2017.

Beven, K. and Germann, P.: Macropores and water flow in soils, Water Resources Research, 18, 1311–1325, https://doi.org/10.1029/WR018i005p01311, 1982.

Bieroza, M. Z. and Heathwaite, A. L.: Seasonal Variation in Phosphorus Concentration-Discharge Hysteresis Inferred from High-Frequency in Situ Monitoring, Journal of Hydrology, 524, 333–347, https://doi.org/10.1016/j.jhydrol.2015.02.036, 2015.

Blom, C. and Voesenek, L.: Flooding: the survival strategies of plants, Trends in Ecology & Evolution, 11, 290–295, https://doi.org/10.1016/0169-5347(96)10034-3, 1996.

Bouchez, J., Gaillardet, J., Lupker, M., Louvat, P., France-Lanord, C., Maurice, L., Armijos, E., and Moquet, J.-S.: Floodplains of large rivers: Weathering reactors or simple silos?, Chemical Geology, 332–333, 166–184, https://doi.org/10.1016/j.chemgeo.2012.09.032, 2012.

https://doi.org/10.5194/egusphere-2026-4826
Preprint. Discussion started: 25 August 2026


Boyer, E., Hornberger, G., Bencala, K., and McKnight, D.: Effects of asynchronous snowmelt on flushing of dissolved organic carbon: a mixing model approach, Hydrological Processes, 14, 3291–3308, https://doi.org/10.1002/1099-1085(20001230)14:18<3291::AID-HYP202>3.0.CO;2-2, 2000.

Bradley, P., Journey, C., Chapelle, F., Lowery, M., and Conrads, P.: Flood Hydrology and Methylmercury Availability in Coastal Plain Rivers, Environmental Science & Technology, 44, 9285–9290, https://doi.org/10.1021/es102917j, 2010.

Buffin-Bélanger, T., Cloutier, C.-A., Tremblay, C., Chaillou, G., and Larocque, M.: Dynamics of groundwater floodwaves and groundwater flood events in an alluvial aquifer, Canadian Water Resources Journal, 41, 469–483, https://doi.org/10.1080/07011784.2015.1102651, 2016.

Burt, T. P., Bates, P. D., Stewart, M. D., Claxton, A. J., Anderson, M. G., and Price, D. A.: Water table fluctuations within the floodplain of the River Severn, England, Journal of Hydrology, 262, 1–20, https://doi.org/10.1016/S0022-1694(01)00567-4, 2002.

Carroll, R. W. H., Bearup, L. A., Brown, W., Dong, W., Bill, M., and Willlams, K. H.: Factors controlling seasonal groundwater and solute flux from snow-dominated basins, Hydrological Processes, 32, 2187–2202, https://doi.org/10.1002/hyp.13151, 2018.

Cey, E. and Rudolph, D.: Field study of macropore flow processes using tension infiltration of a dye tracer in partially saturated soils, Hydrological Processes, 23, 1768–1779, https://doi.org/10.1002/hyp.7302, 2009.

Chanat, J., Rice, K., and Hornberger, G.: Consistency of patterns in concentration-discharge plots, Water Resources Research, 38, https://doi.org/10.1029/2001WR000971, 2002.

Coats, K. and Smith, B.: Dead-End Pore Volume and Dispersion in Porous Media, Society of Petroleum Engineers Journal, 4, 73–84, https://doi.org/10.2118/647-PA, 1964.

Creed, I. F., McKnight, D. M., Pellerin, B. A., Green, M. B., Bergamaschi, B. A., Aiken, G. R., Burns, D. A., Findlay, S. E., Shanley, J. B., Striegl, R. G., Aulenbach, B. T., Clow, D. W., Laudon, H., McGlynn, B. L., McGuire, K. J., Smith, R. A., and Stackpoole, S. M.: The river as a chemostat: fresh perspectives on dissolved organic matter flowing down the river continuum (R. Smith, editor), Canadian Journal of Fisheries and Aquatic Sciences, 72, 1272–1285, https://doi.org/10.1139/cjfas-2014-0400, 2015.

Crosbie, R. S., McEwan, K. L., Jolly, I. D., Holland, K. L., Lamontagne, S., Moe, K. G., and Simmons, C. T.: Salinization risk in semi-arid floodplain wetlands subjected to engineered wetting and drying cycles, Hydrological Processes, 23, 3440–3452, https://doi.org/10.1002/hyp.7445, 2009.

Dam, W. L., Campbell, S., Johnson, R. H., Looney, B. B., Denham, M. E., Eddy-Dilek, C. A., and Babits, S. J.: Refining the site conceptual model at a former uranium mill site in Riverton, Wyoming, USA, Environmental Earth Sciences, 74, 7255–7265, https://doi.org/10.1007/s12665-015-4706-y, 2015.

Day, G., Dietrich, W., Rowland, J., and Marshall, A.: The depositional web on the floodplain of the Fly River, Papua New Guinea, Journal of Geophysical Research: Earth Surface, 113, 2006JF000 622, https://doi.org/10.1029/2006JF000622, 2008.

Dosskey, M. G., Vidon, P., Gurwick, N. P., Allan, C. J., Duval, T. P., and Lowrance, R.: The Role of Riparian Vegetation in Protecting and Improving Chemical Water Quality in Streams, Journal of the American Water Resources Association, 46, 261–277, https://doi.org/10.1111/j.1752-1688.2010.00419.x, 2010.

Ellery, W., Ellery, K., and McCARTHY, T.: Plant distribution in islands of the Okavango Delta, Botswana: determinants and feedback interactions, African Journal of Ecology, 31, 118–134, https://doi.org/10.1111/j.1365-2028.1993.tb00526.x, 1993.

Evans, C. and Davies, T.: Causes of concentration/discharge hysteresis and its potential as a tool for analysis of episode hydrochemistry, Water Resources Research, 34, 129–137, https://doi.org/10.1029/97WR01881, 1998.

https://doi.org/10.5194/egusphere-2026-4826
Preprint. Discussion started: 25 August 2026


Fang, K., Caers, J., and Maher, K.: Modeling continental US stream water quality using long-short term memory and weighted regressions on time, discharge, and season, Frontiers in Water, 6, 1456 647, https://doi.org/10.3389/frwa.2024.1456647, 2024.

Flury, M., Flühler, H., Jury, W., and Leuenberger, J.: Susceptibility of soils to preferential flow of water: A field study, Water Resources Research, 30, 1945–1954, https://doi.org/10.1029/94WR00871, 1994.

Forrer, I., Kasteel, R., Flury, M., and Flühler, H.: Longitudinal and lateral dispersion in an unsaturated field soil, Water Resources Research, 35, 3049–3060, https://doi.org/10.1029/1999WR900185, 1999.

Gale, M. and Grigal, D.: Vertical root distributions of northern tree species in relation to successional status, Canadian Journal of Forest Research, 17, 829–834, https://doi.org/10.1139/x87-131, 1987.

Gerke, H. and Genuchten, M. V.: A dual-porosity model for simulating the preferential movement of water and solutes in structured porous media, Water Resources Research, 29, 305–319, https://doi.org/10.1029/92WR02339, 1993.

Godsey, S., Kirchner, J., and Clow, D.: Concentration–discharge relationships reflect chemostatic characteristics of US catchments, Hydrological Processes, 23, 1844–1864, https://doi.org/10.1002/hyp.7315, 2009.

Hall, F.: Dissolved Solids-Discharge Relationships: 2. Applications to Field Data, Water Resources Research, 7, 591–601, https://doi.org/10.1029/WR007i003p00591, 1971.

Herndon, E. M., Dere, A. L., Sullivan, P. L., Norris, D., Reynolds, B., and Brantley, S. L.: Landscape heterogeneity drives contrasting concentration–discharge relationships in shale headwater catchments, Hydrology and Earth System Sciences, 19, 3333–3347, https://doi.org/10.5194/hess-19-3333-2015, 2015.

Hillel, D.: Unstable flow in layered soils: A review, Hydrological Processes, 1, 143–147, https://doi.org/10.1002/hyp.3360010203, 1987.

Hornberger, G., Bencala, K., and McKnight, D.: Hydrological controls on dissolved organic carbon during snowmelt in the Snake River near Montezuma, Colorado, Biogeochemistry, 25, 147–165, https://doi.org/10.1007/BF00024390, 1994.

House, W. A. and Warwick, M. S.: Hysteresis of the Solute Concentration/Discharge Relationship in Rivers During Storms, Water Research, 32, 2279–2290, https://doi.org/10.1016/S0043-1354(97)00473-9, 1998.

Hurr, R. T.: Ground-water hydrology of the Mormon Island Crane Meadows wildlife area near Grand Island, Hall County, Nebraska, Tech. Rep. 81-1109, U.S. Geological Survey, ISSN 2331-1258, https://doi.org/10.3133/ofr811109, 1981.

Jackson, R. B., Canadell, J., Ehleringer, J. R., Mooney, H. A., Sala, O. E., and Schulze, E. D.: A global analysis of root distributions for terrestrial biomes, Oecologia, 108, 389–411, https://doi.org/10.1007/BF00333714, 1996.

Jarvis, N.: A review of non-equilibrium water flow and solute transport in soil macropores: principles, controlling factors and consequences for water quality, European Journal of Soil Science, 58, 523–546, https://doi.org/10.1111/j.1365-2389.2007.00915.x, 2007.

Javadi, M.: Reactive transport modeling of unsaturated hydrology and geochemistry of neutral and acid rock drainage in highly heterogeneous mine waste rock at the Antamina Mine, Peru, Ph.D. thesis, University of British Columbia, https://doi.org/10.14288/1.0378324, 2019.

Jia, M., Lapen, D., Su, D., and Mayer, K.: Modeling of dual-permeability gas and solute reactive transport in macroporous agricultural soils with a focus on GHG cycling and emissions, Journal of Hydrology, 620, 129 408, https://doi.org/10.1016/j.jhydrol.2023.129408, 2023.

Jia, M., Lapen, D. R., Su, D., and Mayer, K. U.: Multi-Domain Reactive Transport Modeling of GHG Emissions From Macroporous Agricultural Soils With a Focus on $N_2O$ Hotspots and Hot Moments, Water Resources Research, 61, e2025WR040 588, https://doi.org/10.1029/2025WR040588, 2025.

Johnson, N., Likens, G., Bormann, F., Fisher, D., and Pierce, R.: A Working Model for the Variation in Stream Water Chemistry at the Hubbard Brook Experimental Forest, New Hampshire, Water Resources Research, 5, 1353–1363, https://doi.org/10.1029/WR005i006p01353, 1969.

Jolly, I., Walker, G., and Thorburn, P.: Salt accumulation in semi-arid floodplain soils with implications for forest health, Journal of Hydrology, 150, 589–614, https://doi.org/10.1016/0022-1694(93)90127-U, 1993.

Jung, M., Burt, T., and Bates, P.: Toward a conceptual model of floodplain water table response, Water Resources Research, 40, 2003WR002 619, https://doi.org/10.1029/2003WR002619, 2004.

Junk, W. J., Bayley, P., and Sparks, R.: The flood pulse concept in river-floodplain systems, in: Proceedings of the International Large River Symposium, edited by Dodge, D., vol. 106 of *Canadian Special Publication of Fisheries and Aquatic Sciences*, pp. 110–127, 1989.

Knapp, J., von Freyberg, J., Studer, B., Kiewiet, L., and Kirchner, J.: Concentration-discharge relationships vary among hydrological events, reflecting differences in event characteristics, Hydrology and Earth System Sciences, 24, 2561–2576, https://doi.org/10.5194/hess-24-2561-2020, 2020.

Lacroix, E. M., Aeppli, M., Boye, K., Brodie, E., Fendorf, S., Keiluweit, M., Naughton, H. R., Noël, V., and Sihi, D.: Consider the Anoxic Microsite: Acknowledging and Appreciating Spatiotemporal Redox Heterogeneity in Soils and Sediments, ACS Earth and Space Chemistry, 7, 1592–1609, https://doi.org/10.1021/acsearthspacechem.3c00032, 2023.

Lassabatere, L., Yilmaz, D., Peyrard, X., Peyneau, P. E., Lenoir, T., Šimůnek, J., and Angulo-Jaramillo, R.: New Analytical Model for Cumulative Infiltration into Dual-Permeability Soils, Vadose Zone Journal, 13, vzj2013.10.0181, https://doi.org/10.2136/vzj2013.10.0181, 2014.

Looney, B. B., Denham, M. E., and Eddy-Dilek, C. A.: Independent technical evaluation and recommendations for contaminated groundwater at the department of energy office of legacy management Riverton processing site, Tech. Rep. SRNL-STI–2014-00163, 1130785, U.S. Department of Energy Office of Legacy Management, 2014.

Macdonald, D., Dixon, A., Newell, A., and Hallaways, A.: Groundwater flooding within an urbanised flood plain, Journal of Flood Risk Management, 5, 68–80, https://doi.org/10.1111/j.1753-318X.2011.01127.x, 2012.

Maher, K.: The dependence of chemical weathering rates on fluid residence time, Earth and Planetary Science Letters, 294, 101–110, https://doi.org/10.1016/j.epsl.2010.03.010, 2010.

Mayer, K. and MacQuarrie, K.: Solution of the MoMaS reactive transport benchmark with MIN3P—model formulation and simulation results, Computational Geosciences, 14, 405–419, https://doi.org/10.1007/s10596-009-9158-6, 2010.

Mayer, K., Frind, E., and Blowes, D.: Multicomponent reactive transport modeling in variably saturated porous media using a generalized formulation for kinetically controlled reactions, Water Resources Research, 38, 13–1–13–21, https://doi.org/10.1029/2001WR000862, 2002.

Mayer, K., Amos, R., Molins, S., and Gérard, F.: Reactive Transport Modeling in Variably Saturated Media with MIN3P: Basic Model Formulation and Model Enhancements, in: Groundwater Reactive Transport Models, edited by Zhang, F., Yeh, G.-T. G., and Parker, J. C., pp. 186–211, Bentham Science Publishers, 2012.

Mayer, K., Alt-Epping, P., Jacques, D., Arora, B., and Steefel, C.: Benchmark problems for reactive transport modeling of the generation and attenuation of acid rock drainage, Computational Geosciences, 19, 599–611, https://doi.org/10.1007/s10596-015-9476-9, 2015.

McClain, M. E., Boyer, E. W., Dent, C. L., Gergel, S. E., Grimm, N. B., Groffman, P. M., Hart, S. C., Harvey, J. W., Johnston, C. A., Mayorga, E., McDowell, W. H., and Pinay, G.: Biogeochemical Hot Spots and Hot Moments at the Interface of Terrestrial and Aquatic Ecosystems, Ecosystems, 6, 301–312, https://doi.org/10.1007/s10021-003-0161-9, 2003.

McMillan, S. and Noe, G.: Increasing floodplain connectivity through urban stream restoration increases nutrient and sediment retention, Ecological Engineering, 108, 284–295, https://doi.org/10.1016/j.ecoleng.2017.08.006, 2017.

Mertes, L. A. K.: Inundation Hydrology, in: Inland Flood Hazards, edited by Wohl, E. E., pp. 145–166, Cambridge University Press, 1 edn., ISBN 978-0-521-62419-0 978-0-511-52941-2 978-0-521-18966-8, https://doi.org/10.1017/CBO9780511529412.006, 2000.

Meyer Oliveira, A., Van Meerveld, I., Gianasi, F. M., Maciel Silva-Sene, A., Farrapo, C. L., De Carvalho Araújo, F., Oliveira, F., Aparecido Silva Ferreira, L., Carolina Arantes Da Silva, L., Gama Reis, M., Vieira Pompeu, P., and Manoel Dos Santos, R.: Inundation dynamics in seasonally dry floodplain forests in southeastern Brazil, Hydrological Processes, 38, e15 203, https://doi.org/10.1002/hyp.15203, 2024.

Mualem, Y.: A new model for predicting the hydraulic conductivity of unsaturated porous media, Water Resources Research, 12, 513–522, https://doi.org/10.1029/WR012i003p00513, 1976.

Musolff, A., Schmidt, C., Selle, B., and Fleckenstein, J.: Catchment controls on solute export, Advances in Water Resources, 86, 133–146, https://doi.org/10.1016/j.advwatres.2015.09.026, 2015.

Newcomer Johnson, T., Kaushal, S., Mayer, P., Smith, R., and Sivirichi, G.: Nutrient Retention in Restored Streams and Rivers: A Global Review and Synthesis, Water, 8, 116, https://doi.org/10.3390/w8040116, 2016.

Nimmo, J.: The processes of preferential flow in the unsaturated zone, Soil Science Society of America Journal, 85, 1–27, https://doi.org/10.1002/saj2.20143, 2021.

Orozco-López, E., Muñoz-Carpena, R., Gao, B., and Fox, G.: Riparian Vadose Zone Preferential Flow: Review of Concepts, Limitations, and Perspectives, Vadose Zone Journal, 17, 1–20, https://doi.org/10.2136/vzj2018.02.0031, 2018.

Paradis, C., Van Ee, N., Hoss, K., Meurer, C., Tigar, A., Reimus, P., and Johnson, R.: Elucidating mobilization mechanisms of uranium during recharge of river water to contaminated groundwater, Journal of Contaminant Hydrology, 251, 104 076, https://doi.org/10.1016/j.jconhyd.2022.104076, 2022.

Perzan, Z. and Chapin, T.: WellSTIC: A Cost-Effective Sensor for Performing Point Dilution Tests to Measure Groundwater Velocity in Shallow Aquifers, Water Resources Research, 59, e2022WR033 223, https://doi.org/10.1029/2022WR033223, 2023.

Perzan, Z. and Maher, K.: Transport, dispersion, and degradation of nonpoint source contaminants during flood-managed aquifer recharge, Vadose Zone Journal, 23, 1–14, https://doi.org/10.1002/vzj2.20307, 2024.

Perzan, Z., Babey, T., Caers, J., Bargar, J., and Maher, K.: Local and Global Sensitivity Analysis of a Reactive Transport Model Simulating Floodplain Redox Cycling, Water Resources Research, 57, https://doi.org/10.1029/2021WR029723, 2021.

Picel, M. H.: Riverton, Wyoming Processing Site: An Environmental Risk Assessment Update, Tech. rep., Argonne National Laboratory, Lemont, Illinois, 2021.

Rasmussen, A. N., Langenfeld, K., Tolar, B. B., Perzan, Z., Maher, K., Cardarelli, E. L., Bargar, J. R., Boye, K., and Francis, C. A.: Floodplain nitrifiers harbor the genetic potential for utilizing a wide range of organic nitrogen compounds, mSystems, 10, e00 829–25, https://doi.org/10.1128/msystems.00829-25, 2025.

Rezanezhad, F., Price, J. S., Quinton, W. L., Lennartz, B., Milojevic, T., and Van Cappellen, P.: Structure of peat soils and implications for water storage, flow and solute transport: A review update for geochemists, Chemical Geology, 429, 75–84, https://doi.org/10.1016/j.chemgeo.2016.03.010, 2016.

Rose, L., Karwan, D., and Godsey, S.: Concentration–discharge relationships describe solute and sediment mobilization, reaction, and transport at event and longer timescales, Hydrological Processes, 32, 2829–2844, https://doi.org/10.1002/hyp.13235, 2018.

Sawyer, A., Kaplan, L., Lazareva, O., and Michael, H.: Hydrologic dynamics and geochemical responses within a floodplain aquifer and hyporheic zone during Hurricane Sandy, Water Resources Research, 50, 4877–4892, https://doi.org/10.1002/2013WR015101, 2014.

Skaggs, T. H., Poss, J. A., Shouse, P. J., and Grieve, C. M.: Irrigating Forage Crops with Saline Waters: 2. Modeling Root Uptake and Drainage, Vadose Zone Journal, 5, 824–837, https://doi.org/10.2136/vzj2005.0120, 2006.

Sophocleous, M.: Stream-floodwave propagation through the Great Bend alluvial aquifer, Kansas: Field measurements and numerical simulations, Journal of Hydrology, 124, 207–228, https://doi.org/10.1016/0022-1694(91)90015-A, 1991.

Thiros, N., Gardner, W., and Kuhlman, K.: Utilizing Environmental Tracers to Reduce Groundwater Flow and Transport Model Parameter Uncertainties, Water Resources Research, 57, https://doi.org/10.1029/2020WR028235, 2021.

Thompson, S., Basu, N., Lascurain, J., Aubeneau, A., and Rao, P.: Relative dominance of hydrologic versus biogeochemical factors on solute export across impact gradients, Water Resources Research, 47, 2010WR009 605, https://doi.org/10.1029/2010WR009605, 2011.

Tockner, K. and Stanford, J.: Riverine flood plains: present state and future trends, Environmental Conservation, 29, 308–330, https://doi.org/10.1017/S037689290200022X, 2002.

Tolar, B. B., Boye, K., Bobb, C., Maher, K., Bargar, J. R., and Francis, C. A.: Stability of Floodplain Subsurface Microbial Communities Through Seasonal Hydrological and Geochemical Cycles, Frontiers in Earth Science, 8, 338, https://doi.org/10.3389/feart.2020.00338, 2020.

U.S. Department of Energy, O. o. L. M.: Advanced Site Investigation and Monitoring Report of the Riverton, Wyoming, Processing Site, Tech. Rep. S14148, Grand Junction, Colorado, 2016.

van Genuchten, M.: A Closed-form Equation for Predicting the Hydraulic Conductivity of Unsaturated Soils, Soil Science Society of America Journal, 44, 892–898, https://doi.org/10.2136/sssaj1980.03615995004400050002x, 1980.

Weiler, M. and Flühler, H.: Inferring flow types from dye patterns in macroporous soils, Geoderma, 120, 137–153, https://doi.org/10.1016/j.geoderma.2003.08.014, 2004.

White, A. and Brantley, S.: The effect of time on the weathering of silicate minerals: why do weathering rates differ in the laboratory and field?, Chemical Geology, 202, 479–506, https://doi.org/10.1016/j.chemgeo.2003.03.001, 2003.

White, A., Delany, J., Narasimhan, T., and Smith, A.: Groundwater contamination from an inactive uranium mill tailings pile: 1. Application of a chemical mixing model, Water Resources Research, 20, 1743–1752, https://doi.org/10.1029/WR020i011p01743, 1984.

Wight, J. and Hanson, C.: Crop Coefficients for Rangeland, Journal of Range Management, 43, 482, https://doi.org/10.2307/4002349, 1990.

Wohl, E.: An Integrative Conceptualization of Floodplain Storage, Reviews of Geophysics, 59, e2020RG000 724, https://doi.org/10.1029/2020RG000724, 2021.

Xiao, D., Brantley, S., and Li, L.: Vertical Connectivity Regulates Water Transit Time and Chemical Weathering at the Hillslope Scale, Water Resources Research, 57, e2020WR029 207, https://doi.org/10.1029/2020WR029207, 2021.

Zhi, W., Li, L., Dong, W., Brown, W., Kaye, J., Steefel, C., and Williams, K. H.: Distinct Source Water Chemistry Shapes Contrasting Concentration-Discharge Patterns, Water Resources Research, 55, 4233–4251, https://doi.org/10.1029/2018WR024257, 2019.